

NPS ARCHIVE  
1965  
TUCKER, E.

INVESTIGATION OF STRAIN DISTRIBUTION  
AROUND FATIGUE CRACKS IN  
ALUMINUM SHEETS

EDWIN B. TUCKER











INVESTIGATION OF STRAIN DISTRIBUTION  
AROUND FATIGUE CRACKS IN ALUMINUM SHEETS

\* \* \* \* \*

Edwin B. Tucker





INVESTIGATION OF STRAIN DISTRIBUTION  
AROUND FATIGUE CRACKS IN ALUMINUM SHEETS

by

Edwin B. Tucker

Lieutenant, United States Navy

Submitted in partial fulfillment of  
the requirements for the degree of

MASTER OF SCIENCE  
IN  
AERONAUTICAL ENGINEERING

United States Naval Postgraduate School  
Monterey, California

1 9 6 5

PS Archive  
1965  
Tucker, E.

~~T 824~~

Library  
U. S. Naval Postgraduate School  
Monterey, California

DUDLEY KNOX LIBRARY  
NAVAL POSTGRADUATE SCHOOL  
MONTEREY CA 93943-5101

**INVESTIGATION OF STRAIN DISTRIBUTION  
AROUND FATIGUE CRACKS IN ALUMINUM SHEETS**

**by**

**Edwin B. Tucker**

**This work is accepted as fulfilling  
the thesis requirements for the degree of  
MASTER OF SCIENCE**

**IN**

**AERONAUTICAL ENGINEERING**

**from the**

**United States Naval Postgraduate School**



## ABSTRACT

A survey of developments in the field of crack propagation and an experimental investigation of the strain distribution around fatigue cracks in flat aluminum sheets was conducted by Lt. E. B. Tucker, USN, at the Aeronautical Engineering Department of the U. S. Naval Postgraduate School, Monterey, California. Crack propagation was produced by constant stress reverse bending. Crack propagation rates were determined for both central and edge cracks. The nature of the geometry in the thickness direction around the crack tip was described and analyzed with the aid of Newton's Interference Fringes. A possible adaption of the method with the birefringent coating technique is suggested for further study.



## TABLE OF CONTENTS

Section Title	Page
Introduction	1
Part I: Development Trends in the Field of Crack Propagation	1
The Fatigue Crack	1
Elastic Methods	4
Plastic Effects	10
Two Stages of Crack Growth	12
Non-Propagating Fatigue Cracks	15
Dislocation Theory	17
Cumulative Damage in Fatigue	20
Testing Methods	22
Part II: Experimental Investigation of Fatigue Crack Geometry by an Interferometric Method	26
Purpose of Experiments	28
Equipment and Procedure	29
Experimental Results and Discussion	36
Verification of Interferometric Method	36
Crack Propagation Rates	38
Geometry in the Vicinity of a Slowly Growing Crack Under Alternating Loads	39
Crack Geometry Under Tensile Load	43
Slip and Interferometric Fringe Patterns	45
Non-Propagating Fatigue Cracks	46
Photostress and the Interferometric Method	47
Initial Fringe Contours	49
Suggested Areas of Further Investigation	49





<b>Section Title</b>	<b>Page</b>
<b>Conclusions</b>	<b>51</b>
<b>References</b>	<b>53</b>
<b>Tables</b>	<b>76</b>
<b>Appendices</b>	<b>83</b>



## LIST OF ILLUSTRATIONS

Figure	Page
1. Test Specimens	55
2. Reverse Bending Mode Used For Crack Propagation	56
3. Circuit Diagram For Strain Gage Measurements	57
4. Central Slot Crack Propagation Rates	58
5. Edge Slot Crack Propagation Rates	59
6. Central Slot Crack Velocity vs. Applied Stress	60
7. Edge Slot Crack Velocity vs. Applied Stress	61
8. Interference Fringe Intensity With Coated and Uncoated Cover Glass	62
9. Optical System Arrangement	63
10. Fringe Pattern Around a Crack	64
11. Depression Width Measurement	65
12. Fringe Number vs. Crack Length	66
13. Depression Width vs. Crack Length	67
14. Concentric Fringe Contours	68
15. Metal Surface Showing Slip Formation	69
16. Strain Contours Under Tensile Load	70
17. Stress-Strain Curve 2024-T3 Aluminum	71
E-1. Calidyne Shaker Table Equipment	72
E-2. Strain Gage Measuring Equipment	73
E-3. Dillon Testing Machine Arrangement	74
E-4. Optical Equipment Arrangement	75



## INTRODUCTION

Prior to the last fifteen years, details of the behavior of fatigue cracks in metal structures received little attention. Fatigue cracks had been observed in machinery resulting in design trends over the years favoring heavier, stronger structures to ensure longer life under expected working loads. The loads considered were based on the primary endurance limit of the material determined from laboratory specimens. Calculation of maximum allowable loads was possible for simple structures, but complicated assemblies with many joints presented a difficult task of analysis, especially if there was doubt as to the exact value of the applied loads.

Fatigue cracks continued to form in structures that had been very meticulously designed and analyzed. The first attempt to resolve this problem was the concept of a stress concentration factor. The stress concentration factor was an empirical quantity assigned to geometric discontinuities such as rivet holes, welded joints, or notches of the structure. Designs under this concept distributed more of the bulk of the structure to the areas where the stress concentrations were considered present.

Early in the 1950's, a series of catastrophic fatigue failures of the deHavilland Comet aircraft motivated scientists around the world to take a long, hard look into the cause and nature of the failures. Little attention had been paid to the concept of fatigue under alternating loads when the airplane structure was designed. As a result, the





structure failed in flight at a point where the strength had been reduced by fatigue cracks.

One metal used for construction of the Comet was a new aluminum alloy. This alloy and others had been developed for applications where high strength and light weight were requirements such as the rapidly expanding aeronautical industry. However, little was known about its fatigue strength characteristics. This metal was determined to have failed in flight due to fatigue cracking.

A wide range of investigations was started, primary emphasis was on an attempt to develop theoretical expressions for the concentration of stress and the propagation of cracks in thin sheet material.

The measurement methods used for these investigations included mechanical strain gages, electrical strain gages, use of birefringent coatings, and plastic models illuminated with polarized light. Considerable information was gathered for material in the elastic range. Few experiments were conducted in the plastic range of the material because the measuring equipment available was not suitable for taking data in the plastic region.

During the past year, improvement in the quality of birefringent coatings has allowed investigation in the plastic range of some metals. Since a photostress coating provides information on strain components only in the plane of the specimen, a separate method must be used to measure thickness direction strains.





The technique of using Newton interference fringes is a recent development in measuring thickness direction strains. The interference fringe method used for experimental observation presented in this paper has the capability of detecting very small strains in a plastic region as well as around a discontinuity, such as a crack. Other strain devices are unsuitable for use around a crack. Gages that must be attached to the material will not work on a cracked surface and even the new birefringent coatings will not give accurate data at the crack. At present, the interference fringe method appears worthy of further investigation.

In Part I, a general survey of the contributions made by various investigators is presented to familiarize the reader with the current state of developments in the search for an accurate description of the nature of fatigue crack propagation.

In Part II, the results and interpretation of data from an experimental investigation using reverse bending of thin aluminum sheets, and interference fringe measurement of the local residual plastic strains is presented to show one of the many possible avenues of further investigation.



## PART I

### DEVELOPMENT TRENDS IN THE FIELD OF CRACK PROPAGATION

#### The Fatigue Crack

A fatigue crack is a crack that grows under repeated loading. It usually starts at a point of stress concentration. The presence of a notch, seam, rivet hole or welded joint may provide the necessary stress concentration. Under load, the concentration may cause the opening of a small crack. The tip of this crack is of very narrow radius. The sharpness of the crack tip causes an increase in the stress concentration. Under the influence of cyclic loading, the concentration causes crack extension. The crack is thus carried into previously undamaged metal, and the process continues. As the crack develops, more and more stress is present about the tip, the stress concentration increases, and the rate of extension is accelerated. If the stresses are sufficiently high, a critical length is reached and fast fracture occurs. Thus, a propagating fatigue crack is a traveling stress raiser.

The problem of categorizing materials in terms of their ability to resist the initiation and propagation of cracks has many ramifications. A starting point would be to attempt to determine a relation between fatigue crack propagation and the state of stress in the cracked component from the standpoint of the mathematical theory of elasticity.

An initial analysis was developed by Neuber. [3]. His analysis idealizes the material to which it applies by



postulating that it is amorphous, isotropic, and so strong that plastic flow does not occur. This idealization is similar to most analyses that have been developed that apply to elastic phenomena.

In common with most versions of this type of analysis, a stress function is used that ensures the derived stresses are in equilibrium. The use of such a stress function allows boundary conditions to be inserted. In this last respect, his analysis differs from some others in that correct boundary conditions can be inserted while, in the interest of simplicity, other analyses use approximations. [4].

The early work of Griffith [2] on fracture has been the foundation upon which most theories of crack propagation have been built. Griffith assumed the presence of inherent characteristic cracks in glass, which is a perfectly brittle material. These cracks cannot be considered as physical entities since they are calculated to be of sufficient size for visual observation, but they have not been found. For the purposes of analysis, these cracks were assumed to be narrow ellipses with major axes of length  $l$ . Under a nominal stress  $\sigma$  applied normal to such a crack it was shown that the internal energy release per unit thickness

$$U = \frac{\pi \sigma^2 l^2}{4E}$$

would result if the crack developed in perfect material.

At the same time, energy  $W$  would be absorbed by the formation of the crack faces of area  $A$ . The equilibrium conditions

$$\frac{dW}{dA} = \frac{dU}{dA} = \frac{\pi \sigma^2 l_c}{2E}$$





defined a critical crack length  $l_c$  whereupon an increase in stress above the value  $\sigma$  would lead to fracture.

Griffith assumed in the case of glass and similar brittle materials, that if  $l_c$  represented the characteristic "flaw" size, then the condition

$$\sigma_u^2 l_c = \text{constant}$$

expressed the brittle fracture strength  $\sigma_u$ . If it is assumed that the specific surface forming energy  $\left(\frac{dW}{dA}\right)$  remains constant, then the expression

$$\sigma^2 l = \text{constant}$$

could be interpreted as the criterion for fast fracture. It appears that the fracture is sustained by the release of energy in the material.

The Griffith theory considers the material containing a stress field as a continuum, but most engineering materials have a discrete crystalline, molecular or atomic structure. Neuber, in addition to his mathematical hypothesis, attempted to take into account the discrete structure of metals by proposing the concept that the material could be considered as an aggregate of "building blocks" with the property that a stress gradient could not develop across any individual block. The half length of the block can be related to certain mechanical properties of the metal. This leads to an interpretation of the building block as the minimum volume of material, the behavior of which can show a reasonably good correlation with technical strength values. The Neuber "blocks" are similar to the Griffith "cracks" in that they cannot be





considered as physical entities.

A complete analysis and a series of computations for various crack geometries have been presented by Jackson [4] [5] using the Neuber theory. This data is a useful tool for the basic elastic theory values which might be used as a basis for any further investigations.

A basic model of the problem can be simulated by a small notch or slot machined in a thin, flat metal plate. Crack propagation tests could be carried out on the thin sheet with a central crack or with an edge notch, subjected to repeated tensile loads acting in a direction at right angles to the crack. One advantage of the central crack model is that the stress field is symmetrical and adapts itself easier to earlier elastic theory developments.

### Elastic Methods

Rarely in engineering practice can a plane or plate be assumed to be of unlimited size when investigating distribution of stresses. In most cases the dimensions of plates under consideration are not only finite in extent, but quite small. It is necessary, therefore, to determine in which cases the solutions for an infinite plate will be valid for finite plates and yet maintain the required degree of accuracy. It would be best for this purpose to compare results of accurate solutions for both finite and infinite plane surfaces.

Theoretical solutions for isotropic plates of infinite extent have been available for a long time. Muskhelishvili [7] investigated the problem of stress distribution about a



narrow ellipse using a complex transformation

$$Z = \zeta + \frac{K}{\zeta}$$

and the mathematical theory of elasticity. The reason for considering an ellipse was due to the belief that cracks behaved as though there were some finite crack thickness, i.e. a thickness which could be represented by the radius of an imaginary notch. The relations derived from this mathematical analysis contain no limiting assumptions or approximations. Several efforts have been made to accurately describe the stress in a finite plate with varying degrees of accuracy.

Savin [8] investigated the problem of stress distribution around an ellipse in a plate of finite width and infinite length. His method of solution was the superposition of stress functions satisfying the mathematical theory of elasticity such that all boundary conditions were satisfied except for a residual stress at the finite edges. By application of St. Venant's principle, he was able to prove the effect of the residual stresses were negligible a certain distance from the free edge. Another useful but somewhat empirical solution for the finite plate was presented by Westergaard. [9]. His solution used a transformation

$$Z = \frac{\sigma}{\left[1 - \left(\frac{\sin \frac{\pi a}{W}}{\sin \frac{\pi \zeta}{W}}\right)^2\right]^{\frac{1}{2}}}$$

where  $z = x + iy$   
 $w =$  plate width  
 $a =$  crack half length

which satisfies the case of a plate of finite width  $W$  subjected to a uniform stress at its extremities and to distributed variable stresses along the free edges.





By assuming

$$Z = a + Re^{i\theta}$$

an approximate solution is reached. The result shows the infinite plate theory can be used with a correction factor

$$K = \sqrt{\frac{W}{\pi a} \tan \frac{\pi a}{W}}$$

if the crack length is less than half the plate width.

Several other authors have made similar independent efforts to approximate the effect of the finiteness of the plate with results that differ only in terminology. All the attempts used an ellipse as a basic geometrical shape, but different coordinate transformations were used. The complex transformation of Westergaard appeared to have the most sound mathematical basis, and for that reason was described here.

After the sound mathematical basis for a discontinuity in a flat plate was reviewed, the possibility of considering stress intensification in terms of a theoretical stress concentration factor was considered. Assuming only elastic behavior, the nominal stress acting across the net cross section was multiplied by a stress concentration factor derived from the geometry of the discontinuity. The resultant stress distribution for a given external load system provided a reasonable calculation of the ultimate loads necessary to produce static failure. The calculation of the stress concentration factors was further modified by experiment. The resultant concentration factor was an indication of discrepancy between elastic theory and experimental results.



McEvily and Illg [10] developed a stress concentration factor for a crack in a finite sheet starting with the established stress distribution about a circular hole in a finite sheet. For the case of a sheet containing a central symmetrical crack, the stress concentration factor for a circular hole of diameter equal to the total length of the crack was determined. The crack was then considered to be an ellipse of major axis equal to the total crack length. The total stress concentration factor was assumed to be related to that for a hole as follows:

$$K_E = 1 + (K_C - 1) \sqrt{\frac{a}{\rho}} \quad K_C = \text{circle stress concentration factor}$$

where  $K_E$  is the stress concentration factor for the ellipse of semi-major axis  $a$  and tip radius  $\rho$ .

In order to obtain an expression for the stress concentration factor for a crack, the effective radius  $\rho_e$  was substituted for  $\rho$ , where  $\rho_e$  is the effective radius of the fatigue crack; and the crack length was substituted for the major axis of the ellipse.

The final step was to make a correction for "size" effect. Such a correction was made by introducing Neuber's material "block" dimension as follows:

$$K_n = 1 + \frac{K_E - 1}{1 + \sqrt{\frac{\rho'}{\rho_e}}} = 1 + \frac{K_C - 1 \sqrt{a/\rho_e}}{1 + \sqrt{\rho'/\rho_e}}$$

where  $\rho'$  is Neuber's constant determined empirically.

Assuming

$$\rho/\rho_e \approx 1, \quad K_n \approx 1 + \frac{1}{2} (K_C - 1) \sqrt{\frac{a}{\rho_e}}$$

Another stress concentration factor method is proposed by Irwin [11] to obtain correlation between crack propagation





rates. Irwin proposed a stress intensity factor

$$K = \sigma \sqrt{a} \alpha$$

where

$$\alpha = \sqrt{\frac{W}{\pi a} \tan \frac{\pi a}{W}}$$

which is the Westergaard correction for a finite plate,  $a$  is the half length of the crack, and  $w$  is the width of the plate. The basic concept of Irwin's work differs from McEvily and Illg's in that the latter were concerned with ultimate load for static failure and the former was interested in crack propagation rate prior to any ultimate failure. It is of interest to realize the difference in these two concentration factors is at most seven per cent. [12].

It appears the stress required for static failure is a function of the same material parameters as the growth of a crack at stresses less than maximum. It is then reasoned that the same type of mechanism is involved with rapid fracture and the slower growing fatigue crack. Others have presented equivalent stress concentration factors derived from a variety of initial assumptions. Basically, they all follow the premise of the flat plate and an elliptical discontinuity.

Another parameter developed in the attempt to describe phenomena of crack propagation and subsequent fracture is notch sensitivity. The meaning of stress concentration for fatigue strength has led to use of the term "notch" to signify geometric features giving rise to stress concentration effects being considered. This terminology is used since it



is simple, graphic, and devoid of ambiguity.

In general,

$$K_f = \frac{\text{unnotched fatigue strength}}{\text{notched fatigue strength}}$$

does not achieve a value as high as the theoretical stress concentration factor  $K_t$ . In fact, it is customary to consider the deviation of the two as a measure of the response of the material to the "notch" effect on fatigue strength. A convenient parameter of this phenomenon is defined as notch sensitivity

$$\gamma = \frac{K_f - 1}{K_t - 1} \quad [13].$$

The possibility exists of evaluating these factors by means of the theory of elasticity, although the mathematical solutions are quite unwieldy except for simple geometric shapes. Use of digital computers has eliminated the tedium and human error factor and at least one solution is available in numerical form. [4] [5]. This study of the kinetics of fatigue crack propagation, on a macroscopic scale has led to a theory of notch sensitivity which has the particular merit of predicting strength reduction factors in good agreement with experimental values. It should be remembered, the constants outlined by the theory are empirical and one would expect them to be in good agreement with experiment since that is their source.

The stress distribution in a particular geometric form, and under a given loading system, can be established by classical elastic theory with the proviso that derived stress values are elastic and the corresponding strains are





small. In the majority of cases, real metals exhibit plastic deformation prior to fracture, consequently stress concentration studies, while still of great value, assume a modified role when plasticity effects are encountered.

### Plastic Effects

Stresses in excess of the primary yield strength produce plastic strain which in turn, by strain hardening, increases the yield value. The onset of plastic strain changes the linear relationship of stress and strain in the elastic domain and further complicates the stress field through the agency of strain hardening.

One way of viewing the stress distribution near the crack tip is to consider that the material in this region must carry additional load that was previously carried by the material opposite the crack. When plastic flow occurs near the crack tip, the amount of load carried in this area is reduced and the stresses further ahead must increase in order to make up the deficit. In the limit, it could be considered that the region in which plastic flow occurs does not carry any load at all. This can be simulated by removing material at the tip of the notch and examining the redistribution of stress in the remaining material. Thus an upper limit can be defined for plastic effects.

The laws governing plastic and elastic-plastic evolution are based on a series of known facts and on special experiments carried out by Polakowski. [14]. These laws are expressed as follows:



Static or alternating mechanical loading tends to modify the strain hardened state of the material, as reached during its mechanical-thermal history, and to substitute for that original state a new strain-hardened state, independent of the first, which corresponds to the new loading history.

In this connection it should be noted that fatigue hardens a material which is initially mild, but softens a material which has been strain hardened by cold working. Such behavior is extremely important in the case of geometrical notches and of the sharp notch, i.e. a crack. One small volume in the neighborhood of the tip of the notch is subjected to a very high level of stress and therefore is subject to marked plastic evolution during fatigue. Deformations along the borders of this volume are constrained by the remainder of the material which conforms with the theoretical strains described by the theory of elasticity.

Polakowski also stated:

An alternating stress superimposed upon a static stress partly destroys previous work hardening and may promote plastic flow and creep in the direction of the static stress. This fact explains the evolution of initial residual stresses, which tend to disappear under fatigue.

Plastic strain during fatigue takes place at an increasing rate with the intensity of the shear stresses. Such strain plays an important part in the propagation of the crack immediately before each step forward of the crack front. It may also have some effect on the residual static strength of the component, particularly where propagation goes from a lower stress region to an area where stresses are higher. In any case, damage before the appearance of the crack due to repeated plastic deformation becomes greater as plastic





deformation under fatigue increases.

Griffith's energy method of explaining the reason for crack growth has another important feature in the light of elastic and plastic phenomena: a moving crack is one which is fed by the release of stored strain energy.

An additional contribution was presented by Irwin [11] who recognized that unstable crack extension would develop regardless of plastic flow if the plastic strains tended to localize near the boundaries of the crack. He modified Griffith's theory by replacing surface tension with work expended in plastic deformation as the factor controlling fracture. Using this modified expression Irwin showed that a fast moving crack was one which was fed by the release of stored elastic strain energy and was independent of contributions of external loads existing at the time of fracture. The upper limit of fracture velocity in brittle materials is approximately one-third the velocity of longitudinal sound waves in the material. [15].

#### Two Stages of Crack Growth

A recent work in the field of the physical process of fatigue has been carried out by Forsyth. [1]. He shows that there are basically two modes of crack growth, and the change from one to another is a natural division of behavior. The first mode of growth is governed by the local shear stresses, thus cracks will form on those planes most closely aligned with the maximum shear stress directions in the fatigue specimen. The surface grains behave in a soft manner, and cause cracks to start on the surface. There



are several reasons for this. First of all, plastic strain is more rapid at the surface because surface grains have an outer face with low plastic rigidity. In addition, there are geometric irregularities at the surface which produce local stress concentrations. Finally, the surface grains deform more than those in the interior of the metal because the stress usually is maximum at the surface.

The criterion for growth in the second mode is the value of the maximum principal tensile stress operating in the specimen in the region of the crack tip. The transition from mode one to mode two occurs when the ratio of shear stress to tensile stress becomes less than unity as the crack progresses from the surface of the material towards the center of the specimen. This indicates that the peak tensile stress developed across the crack tip causes deviation of the crack from its slip or shear path. Mode two growth contains an element of cleavage. In essence, the crack starts from the surface where the grains will have a lower than average shear strength, then grows into the constrained region of the bulk of the material where cleavage conditions are favored.

Direct observations of surface cracks has been carried out mainly on pure materials especially intended for easy observation in the laboratory. These observations showed that cracks appeared in slip bands and were due to the setting up along these slip bands of zones having unequal rigidity to plastic deformation. It should be noted that a surface strain-hardened condition hinders the full inception





of Forsyth's mode two crack growth due to residual compressive stresses in the material.

Generally speaking, mode two is the most usually encountered mode of crack propagation in construction materials: it accounts for a major proportion of all cracking before rupture or failure. Mode one on the other hand, is the consequence of plastic strain before cracking; the whole mode is in fact governed by the alternating shear stresses. It follows, therefore, that the useful life of the material before the onset of cracking depends mainly on shear stresses.

On examining fatigue fractures in sheets subjected to repeated tensile loadings, it will be seen that quite often crack propagation is intermittent. Each step represents partial static rupture under tensile stress. The static fracture front moves forward faster in the center of the sheet due to the plastic flow near the outer surfaces which locally reduces the applied load. Static fracture stops because its forward motion reduces the stress concentration at the surface of the material. Strain then occurs along the edges of the crack and induce slow propagation which continue until the static rupture phase re-occurs. Final fracture possibly occurs when the increase in local stresses (due to decreasing cross section area) balances reduction in stress concentration due to favorable effect of plastic strain at the surfaces.

Forsyth [1] remarked that when the center of the crack front moves far ahead of the surface position, the

1. The first part of the paper is devoted to a general discussion of the problem of the existence of a solution of the system of equations

$$\begin{cases} \Delta u = f(x, y, z, u, v, w) \\ \Delta v = g(x, y, z, u, v, w) \\ \Delta w = h(x, y, z, u, v, w) \end{cases} \quad (1)$$

in the domain  $D$  bounded by the surface  $S$ , where  $f, g, h$  are continuous functions of the variables  $x, y, z, u, v, w$  and satisfy certain conditions. The second part of the paper is devoted to the study of the properties of the solution of the system (1) in the case when the functions  $f, g, h$  are linear in the variables  $u, v, w$ . The third part of the paper is devoted to the study of the properties of the solution of the system (1) in the case when the functions  $f, g, h$  are quadratic in the variables  $u, v, w$ .

2. In the first part of the paper, we shall assume that the functions  $f, g, h$  are continuous in the domain  $D$  and satisfy the conditions

$$\begin{aligned} &|f(x, y, z, u, v, w)| \leq M_1, \\ &|g(x, y, z, u, v, w)| \leq M_2, \\ &|h(x, y, z, u, v, w)| \leq M_3 \end{aligned}$$

where  $M_1, M_2, M_3$  are positive constants. We shall also assume that the functions  $f, g, h$  are linear in the variables  $u, v, w$ , i.e.,

$$\begin{aligned} f(x, y, z, u, v, w) &= a_1 u + a_2 v + a_3 w + f_0(x, y, z), \\ g(x, y, z, u, v, w) &= b_1 u + b_2 v + b_3 w + g_0(x, y, z), \\ h(x, y, z, u, v, w) &= c_1 u + c_2 v + c_3 w + h_0(x, y, z), \end{aligned}$$

where  $a_1, a_2, a_3, b_1, b_2, b_3, c_1, c_2, c_3$  are constants and  $f_0, g_0, h_0$  are continuous functions of the variables  $x, y, z$ .

3. In the second part of the paper, we shall assume that the functions  $f, g, h$  are quadratic in the variables  $u, v, w$ , i.e.,

$$\begin{aligned} f(x, y, z, u, v, w) &= a_{11} u^2 + a_{12} uv + a_{13} uw + a_{21} uv + a_{22} v^2 + a_{23} vw + a_{31} uw + a_{32} vw + a_{33} w^2 + f_0(x, y, z), \\ g(x, y, z, u, v, w) &= b_{11} u^2 + b_{12} uv + b_{13} uw + b_{21} uv + b_{22} v^2 + b_{23} vw + b_{31} uw + b_{32} vw + b_{33} w^2 + g_0(x, y, z), \\ h(x, y, z, u, v, w) &= c_{11} u^2 + c_{12} uv + c_{13} uw + c_{21} uv + c_{22} v^2 + c_{23} vw + c_{31} uw + c_{32} vw + c_{33} w^2 + h_0(x, y, z), \end{aligned}$$

where  $a_{ij}, b_{ij}, c_{ij}$  are constants and  $f_0, g_0, h_0$  are continuous functions of the variables  $x, y, z$ .

4. In the third part of the paper, we shall assume that the functions  $f, g, h$  are cubic in the variables  $u, v, w$ , i.e.,

$$\begin{aligned} f(x, y, z, u, v, w) &= a_{111} u^3 + a_{112} u^2 v + a_{113} u^2 w + a_{121} u^2 v + a_{122} u^2 w + a_{131} u^2 w + a_{132} u^2 w + a_{133} u^2 w + a_{211} u^3 + a_{212} u^2 v + a_{213} u^2 w + a_{221} u^2 v + a_{222} u^2 w + a_{231} u^2 w + a_{232} u^2 w + a_{233} u^2 w + a_{311} u^3 + a_{312} u^2 v + a_{313} u^2 w + a_{321} u^2 v + a_{322} u^2 w + a_{331} u^2 w + a_{332} u^2 w + a_{333} u^2 w + f_0(x, y, z), \\ g(x, y, z, u, v, w) &= b_{111} u^3 + b_{112} u^2 v + b_{113} u^2 w + b_{121} u^2 v + b_{122} u^2 w + b_{131} u^2 w + b_{132} u^2 w + b_{133} u^2 w + b_{211} u^3 + b_{212} u^2 v + b_{213} u^2 w + b_{221} u^2 v + b_{222} u^2 w + b_{231} u^2 w + b_{232} u^2 w + b_{233} u^2 w + b_{311} u^3 + b_{312} u^2 v + b_{313} u^2 w + b_{321} u^2 v + b_{322} u^2 w + b_{331} u^2 w + b_{332} u^2 w + b_{333} u^2 w + g_0(x, y, z), \\ h(x, y, z, u, v, w) &= c_{111} u^3 + c_{112} u^2 v + c_{113} u^2 w + c_{121} u^2 v + c_{122} u^2 w + c_{131} u^2 w + c_{132} u^2 w + c_{133} u^2 w + c_{211} u^3 + c_{212} u^2 v + c_{213} u^2 w + c_{221} u^2 v + c_{222} u^2 w + c_{231} u^2 w + c_{232} u^2 w + c_{233} u^2 w + c_{311} u^3 + c_{312} u^2 v + c_{313} u^2 w + c_{321} u^2 v + c_{322} u^2 w + c_{331} u^2 w + c_{332} u^2 w + c_{333} u^2 w + h_0(x, y, z), \end{aligned}$$

where  $a_{ijk}, b_{ijk}, c_{ijk}$  are constants and  $f_0, g_0, h_0$  are continuous functions of the variables  $x, y, z$ .

fracture becomes a double bevel making an angle of 45 degrees with the sheet faces. Next, it changes to a single bevel fracture. These changes occur long before crack propagation assumes catastrophic proportions. These 45 degree cracks could be compared with mode one propagation theory. Where plastic strain takes place along a direction of maximum shear stress of 45 degrees at the beginning of a crack, plastic strain is not fully developed and the crack switches to mode two. Later, as plastic strain increases as far as surface grains are concerned, the angle of the crack path gradually becomes 45 degrees. The 90 to 45 degree transition appears unconnected with any variation in crack propagation rate, indicating only local overloads along the shear planes have reached a sufficiently high relative value.

#### Non-Propagating Fatigue Cracks

The phenomenon of non-propagating cracks was commented on by many experimenters who observed it in the course of other investigations. It appeared as a short fatigue crack that seemed to grow fairly rapidly and then stop. A similar and related phenomenon was observed by Hudson and Hardrath [16] during an investigation of changing stress amplitude on crack growth. When the second stress level was lower than the first, two effects of "preloading" became apparent: crack growth was discontinued over a large number of cycles and when crack growth finally started again, it started at a point behind the crack tip. It appeared that residual stresses produced by high stresses at the crack tip were





sufficient to render other portions of the specimen more vulnerable to crack growth at the lower stress level.

The delay phenomenon can also be explained in terms of the residual compressive stresses set up by the higher stress level. The fatigue cycling of the specimen gradually reduces the stresses set up in the crack tip since it is a strain hardened region. When the residual stress is lowered sufficiently, the crack starts to propagate again. If the stress built up at the crack tip is sufficiently high with respect to the subsequent loadings, the amount of stress relief due to fatigue may not be large enough to re-start the crack.

There are essentially two ways in which non-propagating cracks may be formed. If the effective radius of the crack is greater than that of the initial notch due to plastic strain, a decrease in local stress will result and a non-propagating crack will form since the new effective peak stress will be less than the fatigue limit for the material. If the crack closes during the compression portion of the fatigue cycle, a non-propagating crack may also be formed, for the effective range of stress at the tip of the crack would be decreased. The compression of the crack does no damage to the material, in fact it assists in the persistence of the residual compressive stress at the crack tip.

The phenomenon of non-propagating cracks can be explained with reference to Forsyth's two modes of crack growth. The cracks show features that suggest that they start almost immediately as mode two cracks, then grow to a



length at which the crack tip is subject to too small a net tensile stress to continue to grow in this mode. The cracking mode may then change to mode one, characterized by a 45 degree bevel. Because the conditions of constraint are such that easy slip plane growth is impossible, the crack becomes virtually non-propagating. It has been suggested [1] that these cracks do in fact grow very slowly although for all practical purposes they have stopped. This is very likely to be true since the cracks tend to turn over to the shear mode where very small dislocation movements could maintain growth.

#### Dislocation Theory

The observation of slip bands in mineral crystals dates back to 1867, although they were not noticed in metals until 1900. Little further advance occurred until the period 1910-1920 when two important techniques were developed: x-ray diffraction and the ability to grow single crystals in the laboratory. These enabled the structures of metal crystals to be determined, and revealed their characteristic mechanical weaknesses, as well as their modes of deformation.

It was noticed that crystals were made up of lattices of mosaic structure, consisting of blocks of slightly differing orientation. Boundaries between such blocks were composed of arrays of what are called "dislocations". Some calculations on the stresses required to move dislocations were attempted but not until 1947-1948 did the subject start to emerge in coordinated form. [17].





When a fatigue stress is applied to a metal, the individual grains begin to show, after a time, fine slip markings. These consist of slip lines within the material and slip bands on the surface of the material. The number of cycles required to produce these visible slip bands depends on the stress level, but may be several thousand cycles. As stressing continues, some of these bands intensify, possibly only over part of their length, so that such bands do not necessarily extend to the grain boundaries. It is these intense slip bands which appear to be the sources of subsequent fatigue cracks.

Generally speaking, fatigue damage from which a crack is formed is localized near the surface of the specimen. [1]. The cracks start in broad slip bands, traces of which persist during electro-polishing treatments. It is of interest to note that if the slip bands are electropolished to remove the majority of them by the electrolytic erosion, the fatigue life of a specimen may be increased seven fold. [17]. This phenomenon in itself is strong evidence that the nucleus of the fatigue process is located in the slip regions.

Grooves and ridges are formed on the surface of the specimen along the slip bands. The ridges sometimes develop thin tongues of metal called extrusions. The grooves have been named intrusions. In pure fatigue, the cracks seem to start at the surface from intrusions. [18]. The formation of the cracks appears to be a purely geometric process in that they are caused by motion of dislocations in several





intersecting crystallographic planes.

Several dislocation mechanisms have been presented in the last few years to explain the nucleation of fatigue cracks. [17]. For the purpose of this discussion, the exact dislocation mechanism for producing intrusions is not of too much importance. Whatever mechanism is conceived, a general idea of the initial depth of the intrusions can be found from the balance of energies due to new surface produced and the work done by the dislocations or by some other means such as Griffith cracks. [2].

In 1961 Valluri [18] proposed a unified theory of fatigue which included much of the results of previous experimenters explained on the basis of dislocations. The following are the general aspects of his theory.

The fatigue failure of a material was attributed to the growth of a dominant crack. This growth was assumed to occur in jerks and was affected by the hardening characteristics of the material and the range of applied stress. An expression for the growth of a dominant crack as a function of number of cycles was proposed. Failure was assumed to occur when the growing crack became just critical for catastrophic failure at the applied peak tensile stress. Two fundamental equations were derived; one expressing crack growth as a function of number of cycles and the other the number of cycles to failure as a function of peak applied stress. These equations contain five material constants of which three are Young's modulus, the ultimate tensile strength, and the endurance limit. The other two



constants have to be determined from tests. This may be done by determining the S-N curve in fatigue for a number of tests, taking two mean points, and solving for the two constants. If the test points are suitably chosen, the region of validity will be well beyond the 50 to 500,000 cycle range.

Application of the quantitative theory can be used to discuss residual static strength, effect of changing the test stress ratio and the effect of cumulative damage. Some limitations of the theory are pointed out. The nature of the fatigue problem has been attributed to two material variables, grain size and a mean internal stress. This stress, characterized by its mean value, depends on the prior history of the material. Its variation from the mean value and its distribution are not known. It is suggested by Valluri that the fatigue problem will remain statistical in nature because of this.

#### Cumulative Damage in Fatigue

One of the more important practical aspects of the fatigue problem is that of cumulative damage. As the name implies, the problem is concerned with the prediction of the accumulation of damage when a test specimen is subjected to a number of stress pulses either in a regular or a random manner. An extreme case might be acoustical fatigue where stress application may be considered to be simultaneous at a number of different frequencies. Cumulative damage may be treated as an extension of the basic theory of fatigue as proposed by Valluri. [18].





One of the earliest papers published in the field and the most well known is that of Miner. [20]. Miner suggested that the damage at any stress level is equal to the fractional life consumed at that stress level. Thus, if at a stress level  $\sigma_q$  the test specimen has a life of  $N_q$  cycles, and the specimen has been subjected to  $n_q$  cycles, Miner's theory requires that

$$\sum_{q=1}^3 \frac{n_q}{N_q} = 1.$$

This is a fairly reasonable assumption and is extremely simple. This theory however sacrifices two important aspects of experiments. One is the added weight given to higher stresses and the other is the dependence of the order of application of stresses. In order to explain this apparent discrepancy there was introduced the concept that the damage in fatigue might be proportional not to

$$n_q/N_q$$

but to some exponent of it

$$\left[ n_q/N_q \right]^P. \quad [19].$$

According to Valluri's theory [19], the observed features of cumulative damage can be explained with no additional assumptions. The sum of the damage fractions will be very nearly equal to one, only when the stresses are very close to each other. The larger the difference, the greater the departure from the sum of one. Given the stresses and their associated ranges, and the ultimate tensile strength of the material, Valluri derived two equations which provide the slope of "damage lines" for pairs of stresses. These damage lines show the remaining





cycles to failure for the two stresses for either order of application. The slopes of the damage lines are independent of any specific strain hardening mechanism. This seems to indicate that the choice of hardening mechanism has little effect on the response to the order of stressing. This method may be adapted to three or more stress levels, program type loading, or random loading with varying success depending on the statistical confidence of the loadings.

### Testing Methods

The standard experimental technique for plate specimens seems to be the determination of the fatigue load applied to the specimen for the onset of crack propagation initiated at points of high stress concentration. Fine saw cuts, small drill holes, and fusion cracks by electric arcing (Elox) have served as the initial artificial cracks. The methods adopted for measuring crack growth have ranged from direct observation to the use of printed circuits as vernier scales such that propagation breaks the circuit component and operates either a cycle counter or chronometer.

After the crack starts to grow, two general methods of stress application have been used. In one the stress amplitude is maintained constant by reduction of load in proportion to remaining cross-sectional area. The other is maintaining the load amplitude constant, resulting in a gradually increased stress amplitude. One advantage to the constant stress amplitude method is that the rate of crack growth is constant proportional to the original width of the specimen, until final rupture occurs.



There are in existence many practical techniques for analyzing crack growth parameters based on photoelasticity, resistance strain gage surveys and a wide range of mechanical, optical, pneumatic, and electromechanical transducer types of extensiometer. Some of these require complex calculations and analysis before meaningful data can be obtained.

Static residual strength after cracking under fatigue can be determined experimentally in the following two ways: (1) After a crack length  $l$  has occurred under a nominal stress  $\sigma$ , a static test is carried out; this gives a net residual strength  $\sigma_{net}$ . (2) The fatigue test is continued under stress  $\sigma$  up to rupture at  $N$  cycles with a crack length of  $l_r$ . The net stress up to final static rupture is then calculated by

$$\sigma_{r net} = \frac{\sigma}{1 - l_r/w}$$

where  $w$  is the plate width.

Using test procedure (1) above for test specimens of narrow width, a large number of tests carried out on sheets of light aluminum alloy determine the ratio

$$x = \frac{\text{net cracked}}{\text{not cracked}} \quad [12].$$

Using test procedure (2), the static strength varies from 0.14 to 1.0 times the static strength of similar material with no cracking.

Recently Gerberich and Swedlow [21] have developed a photoelastic coating technique which provides separation of the principal plastic strains within a plastic enclave surrounding a crack tip, provided the thickness direction strains are measured by an independent method. Prior to





the development of their method, determination of strains in the neighborhood of the crack tip was not possible due to limitations of the applied coatings. The coatings tended to crack before the metal surface, or to separate from the metal surface around the crack.

The primary requirement for this new technique was the manufacture of a photoelastic coating material: (1) with a strain - optical coefficient,  $K$ , high enough to produce a sufficient number of isochromatics, and (2) flexible enough to avoid premature cracking during the crack propagation tests. The material developed is called epoxy-polysulfide copolymer.

Epoxy-polysulfide copolymer has the unique property of variable elastic modulus, elongation, and strain - optical coefficient dependent on the composition by weight of its component parts. This material may be prepared for use on a wide variety of metals with little difficulty.

In the use of a birefringent coating, a measurement error exists due to the fact that shear values at the metal surface taper off through the thickness of the coating; therefore, calibration of this error is required.

Using this photoelastic coating, values of principal stress difference in the vicinity of the crack were recorded. The strains were computed using a true stress - strain curve for the material in tension, and the fact that for the plastic region,

$$\epsilon_1 + \epsilon_2 + \epsilon_3 = 0.$$





The measurement of thickness direction strain was independently measured by an optical-mechanical comparator allowing thickness estimates of plus or minus 20 microinches.

Further details of the geometry and magnitude of the thickness direction strain distribution around cracks in thin metal sheets were observed with a method utilizing Newton interference fringes. This method was presented by Oppel et al. [22] and holds much promise since strains in the thickness direction can be observed over discontinuities with a minimum of analysis. Further study of this method is indicated for use in conjunction with the photoelastic coating as an accurate method to determine thickness direction strains.

Investigations in this paper will emphasize the area from the crack tip to one specimen thickness away from the tip in an attempt to provide data for use with the birefringent coating method to further analyze the strains close to the crack tip.



## PART II

### EXPERIMENTAL INVESTIGATION OF FATIGUE CRACK GEOMETRY BY AN INTERFEROMETRIC METHOD

As shown in Part I, a considerable amount of information has been presented by numerous authors on the subject of fatigue crack propagation. Various methods have been outlined to attempt prediction of critical crack lengths, rate of crack propagation, character of the propagation, and testing procedures.

One of the areas of interest where little meaningful evidence has been gathered is the plastic enclave around the tip of the growing crack. The reason why investigation in this area has met with only limited success is the fact that no satisfactory methods of observing and recording phenomena at the discontinuity had been developed. The usual strain gages cannot be satisfactorily fastened to the material at the crack. The birefringent materials will determine only two dimensions of the strain when applied to a metal surface which will be cracked. If the coating does not crack along the metal crack, the readings obtained are unusable.

Recently Gerberich and Swedlow [21] developed a technique with a new photoelastic coating that allows separation of the principal strains within a plastic enclave surrounding a crack tip. Suitable coating characteristics for each material tested can be obtained by proper coating composition.

The Newton interferometric method was introduced by Oppel et al. [22] in order to avoid the difficulties experienced with other methods of measurement. The interferometric





method completely avoids these troubles since no coating is used, and in addition permits the observation of strain throughout the entire plastic range of the metal until the specimen is destroyed.



## PURPOSE OF EXPERIMENTS

The purpose of this paper is to investigate the geometry around a fatigue crack using the interferometric method introduced by Oppel. This method consists of observing the interferences formed in the air gap between a plane glass surface placed over and in contact with the specimen, and the polished surface itself. Such an interference pattern provides a contour map of the specimen surface, i.e., the change of thickness of the specimen  $\delta$ . The exact manner in which the measurement is made is described in Appendix 1 where the sensitivity is shown to be (for mercury light)

348  $\mu$  in/in per fringe.

The suitability of this method was verified by comparing results with those calculated for a round hole in an infinite plate using the mathematical theory of elasticity.

The rate of crack propagation was calculated from data taken during fatigue crack growth and compared with results previously published in two independent reports.

The distribution of strain contours around a crack under alternating loads and tensile load was investigated. The shape of the contours was analyzed and discussed.

One specimen with a fully developed fringe pattern was observed without the coated glass to examine the surface of the metal. In the areas where fringe gradient indicated considerable plastic strain, areas of massive slip were observed.



## EQUIPMENT AND PROCEDURE

### Specimens

The test specimens used were 2024-T3 aluminum sheet cut parallel to the roll direction from the same rolled sheet of thickness  $.063 \pm .0005$ . The dimensions of the specimen are shown in Figure 1. A total of fifteen specimens were tested, nine with central slots and six with edge slots. The specimens were carefully polished to a mirror finish across their width at the approximate center on a ten inch cloth wheel using jewelers rouge as a polishing agent. The slots were cut by hand with a jewelers saw with blades .008 and .012 inches wide. The central slots were made by drilling a  $1/16$  inch hole on the centerline and cutting each way with the saw. Nominal length of the slots was .750 inches.

Six of the fifteen specimens prepared for the experimental investigations were selected and designated A-1 through A-6. Table III. These specimens were drilled and reamed for technique suitability tests. After these tests, these six specimens were re-used as central slot specimens by cutting the slot from the reamed hole to a nominal width of .750 with a fine jewelers saw. The slotted specimens were then redesignated specimens 1 through 6. Table I.

The crack propagation tests were performed using all fifteen specimens. The numbers in parentheses in Figures 4 and 5 refer to the specimen numbers for each test recorded in Table I.





The three specimens selected for geometry analysis were specimens 9, 10, and 15. The representative photograph included as Figure 10 and the sketch in Figure 11 were made from specimen 10.

The specimen photographed under tensile load, Figure 16, was an un-numbered specimen used to gain familiarity with the equipment prior to commencing test runs. This un-numbered specimen was the same as the test specimens in which an edge fatigue crack was propagated at 14,600 psi to approximately one half inch. The tensile load was applied to observe the effect on the fringe pattern but the process was discontinued when crack growth under repeated tension was considered too slow to be practical. After the test program was completed, this specimen was included because of the difference in fringe pattern from those shown to be the result of reverse bending.

The crack geometry of three specimens was unique in that concentric circular fringes were observed. These were specimens 7, 8, and 9. See Table V and Figure 13.

A non-propagating crack was produced in specimen 6 during higher level stress application.

### Loading

Symmetrical bending was selected as the mode of load application for several reasons. First of all, there was a Calidyne Model 68 shaker table available with sufficient power to flex the specimens to the desired amplitude. Secondly, the size of the specimen could be selected to cause resonance in bending at a convenient frequency. The



frequency desired was about 60 cps. After machining the specimens to the proper dimensions, the frequency observed was 63 cps. Finally the symmetrical bending caused equal values of tension and compression in the extreme fibers of the specimen with zero mean load. This was desired to eliminate the added complication of a mean static load.

The equation of motion for the natural vibration of an elastic beam cantilevered at one end was solved for the selected specimen. The second mode of vibration was chosen because it created a reasonable value of curvature approximately in the center of the specimen. Figure 2. Details of the calculations are enclosed in Appendix 2.

The values of stress in the extreme fibers were calculated as a function of vibration amplitude which allowed various stress levels to be used by controlling the shaker power output. It is worthy of note that the stress is not a function of plate width, therefore all tests were at constant stress. Six of the specimens tested were equipped with SR-4 type AD-7 strain gages placed longitudinally at the point of maximum amplitude. Strain readings were taken using a standard strain gage bridge circuit. Figure 3. The bridge was DC balanced before start of the readings, then using a Ballantine AC Voltmeter, the strain gage output was recorded in millivolts. Calibration data is included in Appendix 2. The difference between calculated stress and observed stress was less than 3 per cent.

Each specimen was vibrated, using the shaker table, to a predetermined crack length at a set stress level. The





number of cycles was observed using a berkley EPUT meter Model 554-3 which was connected to the shaker output. The shaker was stopped at specific internals during crack growth to measure crack length and number of cycles.

### Crack Propagation

The length of the crack was observed as the distance from the root of the slot to the tip of the crack at the upper surface. Measurement was made with a scale calibrated in 64ths of an inch. All measurements are considered accurate to within one half a scale division or  $1/128$  of an inch. Data taken is recorded in Table I. Crack propagation rates were computed, recorded in Table II, and plotted in Figures 4, 5, 6, and 7.

### Interferometric Method

After each specimen was fatigued, it was wiped clean with acetone. A plane piece of glass  $1/16$  inch thick and one inch by two inches was fastened over the edge of the saw cut covering the fatigue crack. The glass was lightly coated with a silvered layer on the side next to the specimen to increase its reflective capabilities. In order to get the maximum contrast between light and dark fringes, it is necessary that the reflectivity of the polished metal surface and the glass be approximately the same. Figure 4. The interference pattern exists regardless of the amount of coating on the glass, but in order to be seen by the eye the intensity of the light from each surface must be such that cancellation causes dark fringes.



The eye cannot discern variations in light intensity at a high level. The amount of coating required on the glass plate is a function of the type of metal being observed and the degree of polish on the surface. Since the coating process is a relatively easy one, an assortment of cover glass pieces with various coating thicknesses is desirable for selection to obtain optimum fringe contrast.

After the glass had been fastened in place with a small piece of masking tape on each long side, the specimen was mounted in a Dillon Model LW testing machine with a maximum tensile load capability of 10,000 pounds. A mercury arc source with a Wratten type 74 filter illuminated the specimen using a reflecting glass which was positioned to direct the light onto the specimen and into the eyepiece of a Gaetner Scientific Company 30 power microscope. Figure 9. The microscope was adjustable to allow observation of the entire area around the crack. A polaroid camera back was fitted with a fixed focus shutter and aperture assembly from another camera. The lenses were removed from the shutter assembly and the microscope lenses used to focus the image on the film. The camera assembly was made removable so the crack could be observed carefully and photographs made of items of interest. Selected photographs and sketches of strain contours are included in Figures 10 to 16.

#### Verification Method

To verify the accuracy and suitability of the interference fringe measurement method, a series of tension tests were run on a known discontinuity. Six polished specimens





were prepared from the available fatigue specimens. A round hole was drilled in the center and carefully reamed to .067 inches. The specimens were inserted in a visual comparator with a magnification of 30. The holes were found to be round within plus or minus .0005 inches. The specimens were mounted in the Dillon machine, a load of 2785 pounds applied, and the specimen observed through the microscope. As the load was slowly removed, the number of fringes was counted moving past eight selected points on the hole circumference where stress level was known.

The verification setup was designed to measure the number of "moving" fringes past a reference point so that net strain was obtained. Using this method, the initial and final strain patterns were not important and did not have to be analyzed.

The maximum stress at the hole was 32,900 psi which is well below the yield point for the material. At this magnitude of load, the fringes are quite wide and are of uneven width. An extremely sensitive feature of this testing method is the placement of the specimen in the Dillon machine. A very small amount of twisting can cause a large change in the number of fringes observed.

The jaws of the Dillon machine were quite flexible to allow specimen alignment before applying tension. The fit of the jaw assemblies to the machine allowed rotation of the lower jaws during application of the first 500 pounds of load. This twist could be prevented by applying about 300 pounds, carefully aligning the specimen, loading to 500





pounds, and realigning the jaws with a wrench until the fringe pattern observed was free of diagonal fringes.

The Dillon machine is not considered practical for an extended tensile test program using the interferometric technique for observations due to the time consuming process necessary to align the specimen. A larger, more stable machine with a yoke and at least two tension screws would be satisfactory for this purpose. Due to the time element involved, investigation with another tension machine was not practical. The results of the accuracy tests are presented in Table III. The stress calculations are included in Appendix 3.

#### Direct Observation of Metal Surface

Specimen 15 was positioned under the microscope without the coated glass to observe the physical nature of the metal surface. In the areas where fringe gradient indicated considerable plastic strain, areas of massive slip were observed. Figure 15.



## EXPERIMENTAL RESULTS AND DISCUSSION

### Verification of Interferometric Method

The analytic solution for the stress distribution around a circular hole in an infinite plate enclosed in Appendix 3 is derived from the superposition of two linear components. The two parts were considered to be: (1) a thin disc whose diameter was equal to the width of the plate with a central hole equal to the reamed hole in the specimen, and (2) a solid disc of the same diameter with no hole. The disc with hole was assumed to be subjected to a constant radial stress of  $S/2$ . The solid disc was assumed to experience both a radial and tangential stress which were functions of angular position.

A stress function satisfying equilibrium conditions was invented for each part. Appropriate boundary conditions were used to evaluate the integration constants for the case of the solid disc. Strain-displacement restrictions and compatibility relations were employed in addition to boundary conditions to evaluate the functions of integration and constants of integration for the case of the disc with the hole. The superposition of these two solutions accurately describe the stress conditions in the plate as a function of angular position and distance from the hole. If the hole diameter is very small compared to the plate width, no detectible error is involved due to the finite plate width. The expressions for stresses at the circumference of the hole are

$$\sigma_r = 0, \quad \sigma_\theta = S[1 - 2 \cos 2\theta]$$

where  $S$  is the applied stress.





The points of interest around the circumference were taken where the stress was equal to  $3 S$ ,  $-S$ , and zero. The stress is equal to  $3 S$  at plus or minus 90 degrees from the direction of the applied stress. The stress is equal to minus  $S$  at a position parallel to the applied stress, and is zero at an angle of 30 degrees from the direction of applied stress. It was determined that a stress of 10,950 psi would cause passage of one fringe on the specimen far from the hole. Appendix 3. The term "far from the hole" is defined to be a sufficient distance from the stress raiser such that the stress measured is the average stress in the specimen if no hole were present.

The six specimens were observed as the stress was applied and the number of fringes passing each point of interest on the circumference of the hole was recorded in Table III. In the table, plus and minus signs denote partial fringe motion too small to measure accurately. They are included to increase confidence in interpreting the data since all values are very small numbers. This technique is not intended as a proof of the calculation method, but to indicate a definite correlation between the calculated strains and the number of fringes observed.

On the basis of the correlation between the calculated and observed results for a known stress and strain distribution, the observation of strain patterns around cracks by this method is considered satisfactory. A more rigorous calibration might be obtained by increasing the load level on the calibration specimens in order to produce passage of



more fringes and lessen the effect of specimen twist in the tension machine.

Care must be taken not to approach the yield point for the material as the plastic strains involved would create errors in the readings. Yield stress for 2024-T3 aluminum is about 48,000 psi. Yield stress is defined by a permanent strain of 2,000 microinches per inch, or about six fringe orders. It is therefore recommended that stresses on the order of 30,000 psi be employed only if lower stress levels are considered unsatisfactory.

#### Crack Propagation Rates

Although the main purpose of this paper is to examine the strain distribution around the fatigue crack, it was decided to verify the rate of crack growth by careful measurement of the crack length at regular intervals during fatigue cycling. The data was presented in Table I for both edge cracks and central cracks. The measurements were made using a steel scale calibrated in sixty-fourths of an inch with the specimen under a strong light. The curves of crack length versus cycles shown in Figures 4 and 5 show linear growth of the cracks at each stress level. The numbers at the end of each curve indicate the specimen number of that curve. The rate of crack growth for each stress was recorded in Table II and plotted in Figures 6 and 7.

The curves show the rate of growth for both types of crack to be proportional to the fifth power of the applied stress. The rate of growth of the central cracks was almost





exactly half the rate for edge cracks. Appendix 4. Considering that there was an equal amount of energy applied to both types of specimens at the same stress level, it follows that the central crack propagation rate would be half the edge crack rate because two cracks were growing simultaneously. The propagation rates observed compare favorably with data presented by Frost and Dugdale [1], and McEvily and Illg [10]. The slope of the curve of growth rate as a function of stress with alternate tension and compression at the stress levels used was determined to be

$$\frac{dl}{dN} = K \sigma^{5.09}$$

by Frost and Dugdale, and

$$\frac{dl}{dN} = K \sigma^{4.95}$$

by McEvily and Illg.

#### Geometry in the Vicinity of a Slowly Growing Crack Under Alternating Loads

Three specimens selected for analysis were photographed along the length of the fatigue crack. A representative photograph is included. Figure 10. The outstanding characteristic of most crack pictures was the formation of fringes parallel to the crack indicating a depression in the metal through which the crack grew. This depression appears to be formed by the plastic deformation at the tip of the crack due to local stresses above the yield stress for the material.

When the material experiences a local stress sufficient to produce fracture, the crack grows slightly and stops. [18]





When stress again is increased to produce fracture, the crack tip moves on, but the depression caused by plastic strain remains. Once the crack tip has passed, the load in the material each side of the crack decreases. The depression around the crack appears to be evidence of the local stresses causing the crack to propagate. Measurements were made of the width of the depression and the number of fringes contained in the depression at intervals along the crack. These measurements are recorded in Table IV and presented in Figure 13.

The width of the depression was measured from the point on one side of the crack where the fringe contours changed direction to a point on the other side where the same direction change occurred. It must be emphasized that the measurement of width might vary with interpretation of the observer as to just what constitutes a direction change. For qualitative observations a consistent interpretation will suffice to establish a trend.

More accurate observations would be realized if the specimen were observed periodically during its growth and the change in fringe pattern recorded. A comparison of successive photographs should pin down the location of the direction change.

The number of fringes contained in the depression was counted across the full width of the depression for two reasons. The crack was not always in the center of the depression, but shifted from side to side as it grew, riding up the slope of the depression at the surface when shear



fracture predominated and favoring the center during cleavage fracture as indicated by Forsyth. [1].

The general fringe field observed on the specimens was not always perpendicular to the crack direction, but at an angle. Counting fringes over the full depression width tended to eliminate any errors due to the slanted fringe field. Any additional fringes counted on one side due to this angle would be balanced by a shortage of fringes on the other side of the crack. Figure 11.

The rate of increase in depression width appears to be higher for the higher applied stress. A possible explanation would be that the higher stress, while causing a higher propagation rate, also causes a greater amount of plastic strain of the material.

The number of fringes observed in the depressions appeared to increase at the same rate as the width of the depressions, indicating a relatively constant gradient to the depression. Observation of the crack tip in Figure 10 shows the depression reaches its full width after the tip passes. The contour of the depression is swept back along the direction of crack growth. This might be caused by stresses behind the crack tip of still sufficient magnitude to be above yield stress for the material.

The fringe contours observed were readily repeatable under subsequent attachment of the coated cover glass if care was taken to ensure both surfaces were clean. This would tend to indicate the appearance of the contours is not particularly sensitive to cover glass placement and









the familiar parallel fringes became evident.

After the parallel fringes became the dominant feature, it was noticed they decreased in width where a small series of circular fringes was observed. This pattern may be explained by a stoppage of the crack at the position of the concentric circles followed by a rapid fracture that did not plastically deform the surrounding surface material in the thickness direction.

The overall rate of propagation was not significantly different for these specimens than others at the same stress level, indicating a possible change in form of the available energy, but an essentially uniform energy release rate.

Another possibility is that the majority of the plastic deformation shifted to the underside of the specimen which was not observed. Unfortunately, no method was available to investigate this because the under surfaces had not been polished before fatiguing the specimens.

If an attempt had been made to polish the reverse sides of the specimens, after the crack was formed much of the strain detail would have been polished off. No conclusive statements can be made concerning the formation of concentric fringes because only a few specimens evidenced this phenomenon. An intensive testing program might reveal more details, particularly if information were available on strains in all three dimensions.

#### Crack Geometry Under Tensile Load

The previously cracked specimen loaded in tension and photographed in Figure 16 indicates a radical change in the



fringe pattern from that of the crack fatigued in alternate tension and compression. Figure 10. After eleven cycles of load, a large circular depression was formed around the crack tip at 2,000 pounds load, corresponding to 10,600 psi. Comparison with the pattern under no load shows an almost identical pattern, indicating most all of the observed strain was permanent deformation caused by plastic strain during previous load cycles. Observation of the photograph under no load condition reveals the fringes along the crack tending to become more parallel to the crack. It is possible that this shows the mechanism whereby the depression is formed along a growing crack.

When alternate tension and compression is applied to a specimen, it appears reasonable to assume much of the circular deformation at the tip of the crack is relieved, leaving the parallel fringes behind the crack tip relatively undisturbed.

A well defined theory on this subject has been presented by Valluri [18] wherein he explained the process of building up residual compressive stresses due to strain hardening from repeated tensile loads. Valluri stated that the deformation takes on the character of a hysteresis loop oriented on the positive side of the  $\sigma - \epsilon$  axes where positive convention is tensile stress and elongation. After several repeated tensile loads the state of the material became one of local compression under no load. The hysteresis loop was then partly compressive and partly tensile.





If the applied loads were alternating compression and tension in reverse bending, the loop was not formed. Residual compressive stress after a tension cycle was almost completely removed by the following compressive cycle. The result was very little residual strain ahead of the crack.

The fringes appeared to line up parallel to the crack behind the tip, possibly because the material experienced tension when it was applied but did not feel the compression until the crack was closed. This environment of more tension than compression might possibly lead to the state of strain observed after the crack had been propagated in symmetrical reverse bending.

A recommended procedure might be to observe a specimen after each tensile load application and record the number of tensile cycles to produce a residual circular enclave of a certain dimension in an effort to determine the characteristics of the enclave formation. Additional data might be obtained by applying individual compressive cycles as well to observe their effect on the established enclave. Equipment was not available during this investigation to apply single compressive loads, so no further evidence could be presented to support this possibility.

#### Slip and Interferometric Fringe Patterns

One specimen with a fully developed fringe pattern was observed without the coated glass to examine the surface of the metal for evidence of slip in the zone of plastic deformation. Specimen 15 was chosen because it evidenced a wide deformed area with the crack well towards one side.



A photograph of the metal surface is enclosed in Figure 15. The increasing area of deformation is below the crack.

Although the 30 power microscope is of much lower power than those used for metallurgical observations, a large area of oriented deformation is visible. The areas of massive slip are identified by bands of closely spaced lines at an approximate 45 degree angle from the crack direction. It is assumed that if the material were properly polished, etched, and observed under higher magnification, that the areas of slip would be very much more pronounced. Evidence of slip in the area of deformation where fringes are pronounced indicates a connection between the slip and plastic strain in the material as stated by Forsyth [1], Valluri [18], et al.

#### Non-Propagating Fatigue Cracks

During the fatigue testing of Specimen 6 at a relatively high stress level (29,300 psi), the reverse bending was stopped to make a crack length measurement. When reverse bending was reapplied, the amplitude was inadvertently raised to a stress level of 40,000 psi for about 100 cycles. The stress level was immediately readjusted. When the next length measurement was made, the initial crack had stopped and a new crack had started about 13/32 behind the tip of the original crack.

The reason for this phenomenon has been explained by Hudson and Hardrath [16] as due to residual compressive stresses set up by the higher stress level. When fatigue was reapplied at the lower level, it gradually reduced the





stresses set up in the vicinity of the first crack tip. The stresses at a point behind the crack tip were lower than at the tip, and would be relieved down to a stress level to permit growth before the tip area. The orientation of the two cracks was identical to [16], Figure 6. No significant change in growth rate was observed after the new crack started.

#### Photostress and the Interferometric Method

No actual tests were made with birefringent coatings in conjunction with the measurement technique described. The photostress method outlined by Gerberich and Swedlow [21] is particularly adaptable to the interferometric method for the following reasons. Gerberich indicated the specimens used were polished before application of the birefringent coating. After the crack was propagated the coating and adhesive were removed in order to measure thickness direction strain at specified grid points with an optical-mechanical instrument.

The striking advantage of the interferometric technique is that it presents a continuous field of thickness contours. Point by point measurements on a grid are not only tedious, but subject to considerable error due to the fact that the measuring instrument must be moved to view each grid point separately, or the specimen must be moved relative to the measuring instrument. The fringe method shows thickness contours over the entire field of view at one setting. The contours are simple to analyze and required calculation to convert directly to strains are brief.



The interferometric technique could be employed using the polished surface of the specimens described. Another advantage is that direct observations could be made at the crack tip. With accurate thickness strains available at the tip, the photostress isochromatics could be interpreted much more closely to the discontinuity. Since

$$\epsilon_2 = \epsilon_3 = -\frac{1}{2}\epsilon_1$$

at the free boundary (Appendix 1), direct calculation there of all three strains is possible. Since with suitable coating thickness, strains may now be measured very close to the crack tip, the interferometric method data overlaps that obtainable by photostress methods. This fortunate state of affairs might well provide better information surrounding the crack tip.

The interferometric method is also useable with little loss in accuracy at large distances from the crack tip where other photostress coatings give accurate readings. Loss in accuracy of the interferometric method far from the crack is due to widening of the fringes as the strain gradient becomes shallow. The precision with which fringe orders can be determined becomes correspondingly less since the exact center of a wide dark fringe with erratic edges is somewhat subject to interpretation of the experimenter. With measurements at these two extreme conditions available, it is suggested further work might be justified in attempting to join the two regions of known data with much more confidence than is now possible.





## Initial Fringe Contours

Throughout this discussion no mention has been made of the interferometric fringe contours under no load before fatigue loading was applied. The initial contours depend on the flatness of the uncracked specimen and the flatness of the "plane" cover glass used. The flatness of the specimen is dependent on the nature of its manufacture which might cause bending, warping, etc; and the nature of the polished surface. It is felt that the magnitude of such initial strains are small compared to the strains around the crack and pose no serious problem. The nature of this investigation was primarily qualitative so no attempt was made to record initial condition strains.

It is expected that a machining burr or foreign body would occasionally get between the polished surface and the cover glass. This condition is readily observable and can be avoided by trying a different orientation of the cover glass, a thorough cleaning of the specimen with acetone, or other suitable solvent. In addition, the nature of the depression around a crack appears to be a relative thing that has little bearing on the initial uncracked contours.

## Suggested Areas for Further Investigation

(1) The initial calibration of the interferometric technique might better be performed at a higher stress level producing the passage of more fringes past the observed point.

(2) Crack geometry observation might produce more information if a series of photographs were taken at





specific intervals during crack growth.

(3) The polishing of both sides of each specimen before fatigue would allow observation of both sides of each crack for changes in depression geometry.

(4) Observations after each tensile cycle in the Dillon machine might reveal the number of cycles to produce a depression of a given size. The application of a compressive load would allow observation of change in depression shape with alternate tension and compression.

(5) A testing program combining the interferometric technique with the application of photoelastic coatings is suggested to further observe the strains around cracks in sheet materials.



## CONCLUSIONS

(1) The interferometric method of thickness direction strain observation seems satisfactory. No significant error was observed when this method was used to determine strains around a circular hole in an "infinite" plate and compared with an analytic solution.

(2) Compatibility of the interferometric method with a photoelastic coating technique developed by Gerberich and Swedlow [21] was suggested. This optical method may provide more thickness dimension strain data for use with the coating isochromatics to better describe conditions at the tip of a fatigue crack.

(3) The width of the plastic strain depression through which the crack grew appeared to be a function of the length of the crack and the magnitude of the applied stress. The slope of the plots of depression width versus crack length were linear over most of the crack length. The gradient of the depth of the depression appeared constant with crack length.

(4) Under tensile loading the character of the contour lines changed to a circular shape. After a specimen had been cycled eleven times at a load of 2,000 pounds, there was little difference in the loaded and unloaded contours indicating the strain observed was possibly mostly permanent plastic deformation. It was suggested that the reverse bending tension and compression considerably reduced this circular shape ahead of the crack tip and caused the parallel fringes along the crack to become the dominant feature.





(5) During reverse bending at lower stress level, the character of the fringes was observed to be concentric contours spaced along the crack with little evidence of strain between them. It was suggested this was caused by stoppage of the crack causing the concentric contours followed by rapid fracture. Further testing in this direction was suggested.

(6) Crack propagation rates for all specimens tested could be expressed by the relation

$$V = K \sigma^5$$

where  $V$  is length per cycle,  $K$  is a constant proportional to plate width, and  $\sigma$  is the net stress applied to the specimen. For central cracks the rate was one half the rate for edge cracks because two cracks were growing, one from each edge of the initial slot.

(7) One non-propagating fatigue crack was inadvertently created which appeared identical to one presented by Hudson and Hardrath [16] during their investigation of specimen reaction to two stress levels.

(8) One specimen with a fully developed fringe pattern was examined without the coated glass. Evidence of massive slip in the depression around the crack tip was indicated, conforming to results presented by Forsyth [1] and Valluri [18].



## References

1. Crack Propagation Symposium, Cranfield College of Aeronautics, Cranfield, England, 1961.
2. Griffith, A. A., Phil. Trans. Roy. Soc. A Vol. 221, 1920.
3. Neuber, H., "Kerbspannungslehre", Second Edition, Julius Springer, Berlin, 1958, Office of Technical Services, Dept. of Commerce, Translation Number AEC-tr-4547.
4. Jackson, R. L., Some Observations on the Distribution of Stress in the Vicinity of a Crack in the Center of a Plate, Defense Metals Information Center, Battelle Memorial Institute, Columbus 1, Ohio, DMIC Memorandum 178, Sept. 18, 1963.
5. Jackson, R. L., Continued Observations on the Distribution of Stress in the Vicinity of a Crack in the Center of a Plate, Defense Metals Information Center, Battelle Memorial Institute, Columbus 1, Ohio, DMIC Memorandum 190, April 14, 1964.
6. Wood, W. A., and Rachinger, W. A., Crystalline Theory of Strength of Metals, Journal of the Institute of Metals, 75, 1949.
7. Muskhelishvili, M. I., A New General Method of Solution of the Fundamental Boundary Problems of the Plane Theory of Elasticity, Dokl. Akad. Nauk SSSR, III, No. 3, 141 (1934).
8. Savin, G. N., Stress Concentration Around Holes, Pergamon Press, New York, Oxford, London, Paris, (1961)
9. Westergaard, H. M., Journal of Applied Mechanics, 6, 1939.
10. McEvily, A. J. Jr., and Illg, W., The Rate of Fatigue Crack Propagation in Two Aluminum Alloys, NACA TN 4394, Sept. 1958.
11. Irwin, G. R., Fracture Mechanics, Structural Mechanics- Proceedings of the First Symposium on Naval Structural Mechanics, Stanford University, Palo Alto, California, August, 1958, Pergamon Press, New York, Oxford, London, Paris, 1960.
12. Barrois, W., Critical Study on Fatigue Crack Propagation, AGARD report 412, June, 1962.
13. Harris, W. J., Metallic Fatigue, Pergamon Press, New York, Oxford, London, Paris, 1961.





14. Polakowski, N. H., Softening of Metals During Cold Working, Journal of the Iron and Steel Institute, December, 1951.
15. Roberts, D. K., and Wells, A. A., The Velocity of Brittle Fracture, Engineering, No. 4639, 1954.
16. Hudson, M. C., and Hardrath, H. F., Effect of Changing Stress Amplitude on the Rate of Fatigue Crack Propagation in Two Aluminum Alloys, NASA TN-D-960, September, 1961.
17. Kennedy, A. J., Processes of Creep and Fatigue in Metals, John Wiley and Sons, Inc., New York, 1963.
18. Valluri, S. R., A Unified Engineering Theory of High Stress Level Fatigue, California Institute of Technology, Pasadena, California, Dec., 1961, ARL 181.
19. Valluri, S. R., A Theory of Cumulative Damage in Fatigue, California Institute of Technology, Pasadena, California, Dec., 1961, ARL 182.
20. Miner, M. A., Cumulative Damage in Fatigue, Journal of Applied Mechanics, Sept., 1945.
21. Gerberich, W. W., and Swedlow, J. L., Plastic Strains and Energy Density in Cracked Plates, Experimental Mechanics, November, 1964.
22. Oppel, G. U., Hill, P. W., and Richter, H., Research Investigation on Strain Analysis of Metal Sheets with Notches and Cracks, Aeronautical Research Laboratory report ARL-317, March, 1962.
23. von Karman, T., and Biot, M. A., Mathematical Methods in Engineering, McGraw-Hill, New York, 1940.
24. Timoshenko, S. and Goodier, J. N., Theory of Elasticity, Second Edition, McGraw-Hill Book Co., Inc., New York, 1951.
25. Sears, F. W., Optics, Addison-Wesley, Cambridge, Mass., 1938.
26. Tolansky, S., An Introduction to Interferometry, Longmans, Green and Co., London, 1955.
27. Sears, F. W., and Zemansky, University Physics, Addison-Wesley, Cambridge, Mass., 1955.



THE UNIVERSITY OF CHICAGO

THE DIVISION OF THE PHYSICAL SCIENCES

DEPARTMENT OF CHEMISTRY

RECEIVED

FROM

DATE

BY

REMARKS

ANALYST

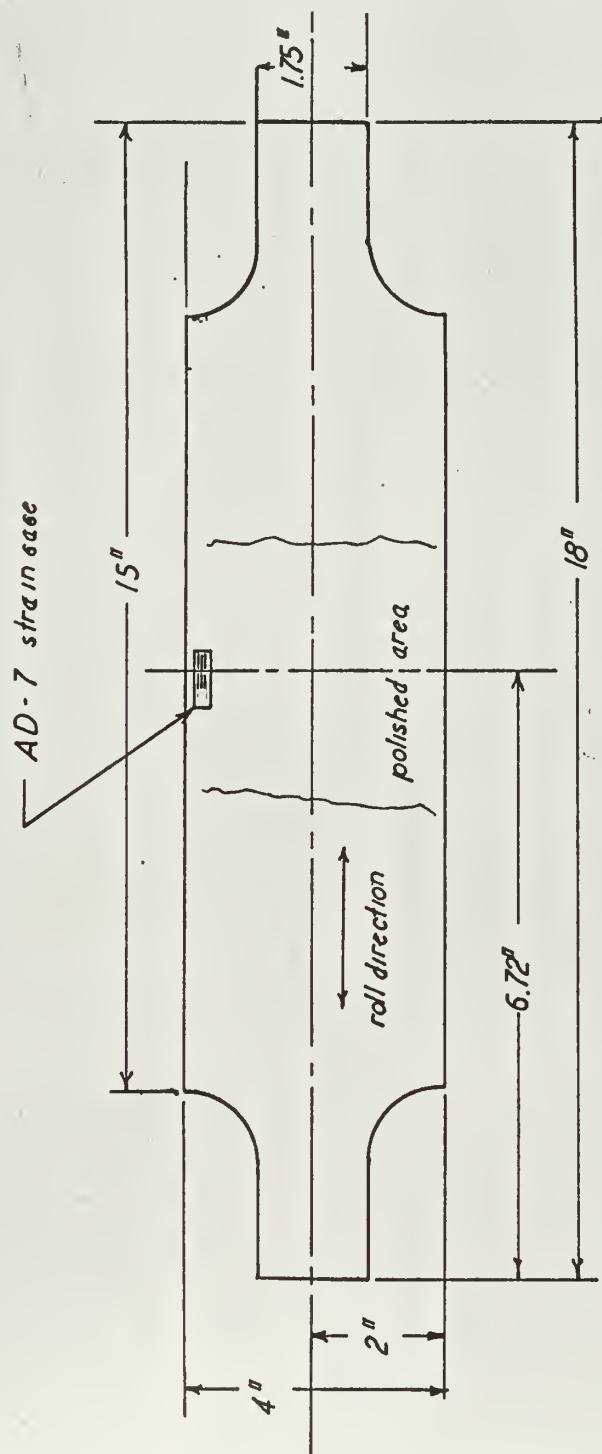
EXAMINER

DATE

BY

REMARKS

ANALYST

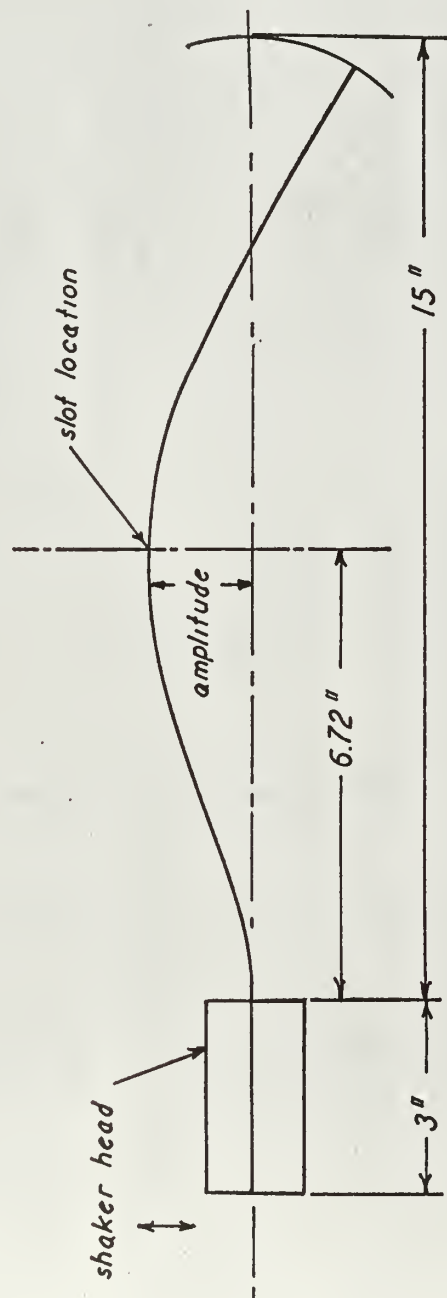


TEST SPECIMENS

.0625 Aluminum Sheet

FIGURE 1





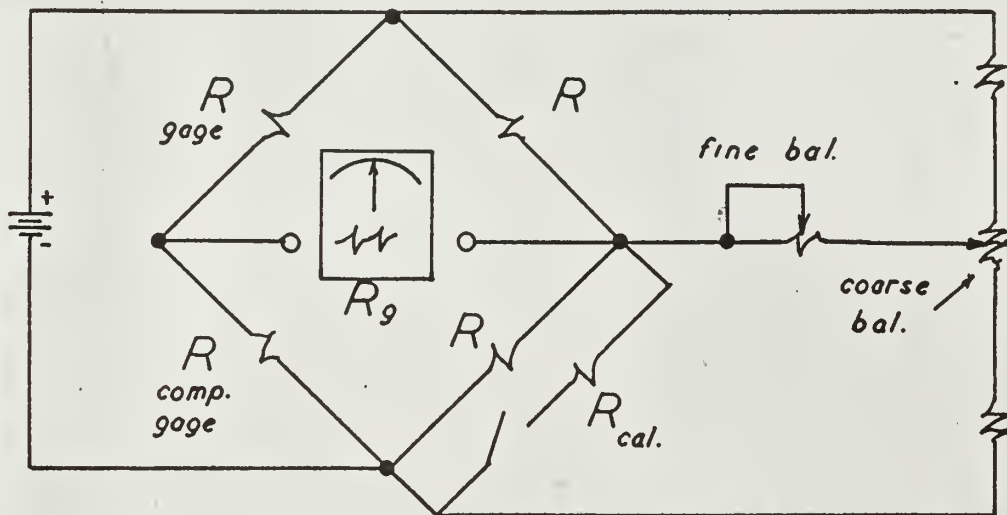
REVERSE BENDING MODE USED FOR  
CRACK PROPAGATION

FIGURE 2





CIRCUIT DIAGRAM  
FOR STRAIN GAGE MEASUREMENTS



$$R_{cal.} = 60 K \Omega$$

$$SENS. = \frac{3 \text{ mv.}}{1000 \mu\%}$$

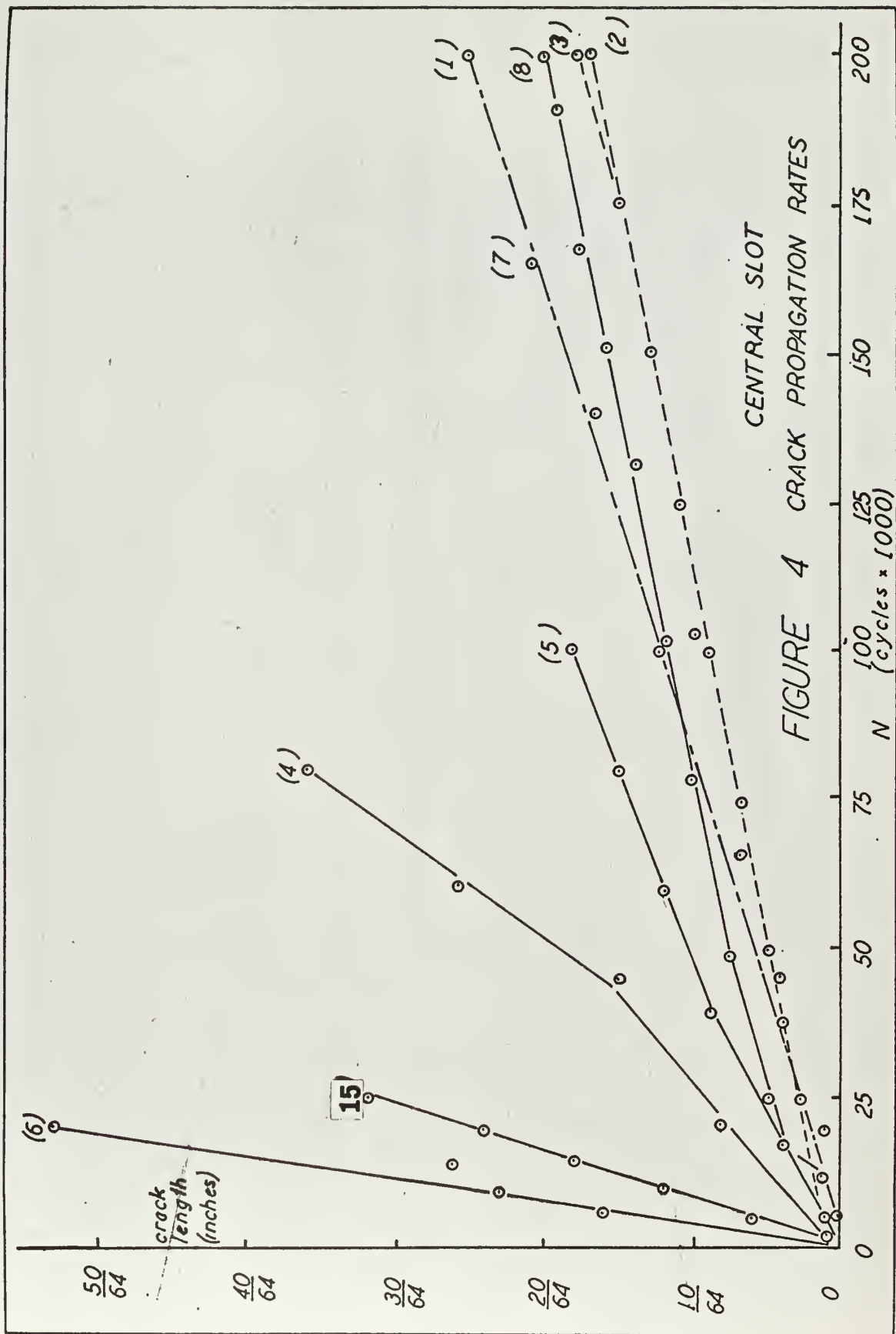
$$E_{out (peak)} = E_{out (rms)} \times 1.414$$

$$472.0 \times E_{out (rms)} = \text{STRAIN } (\mu\%)$$

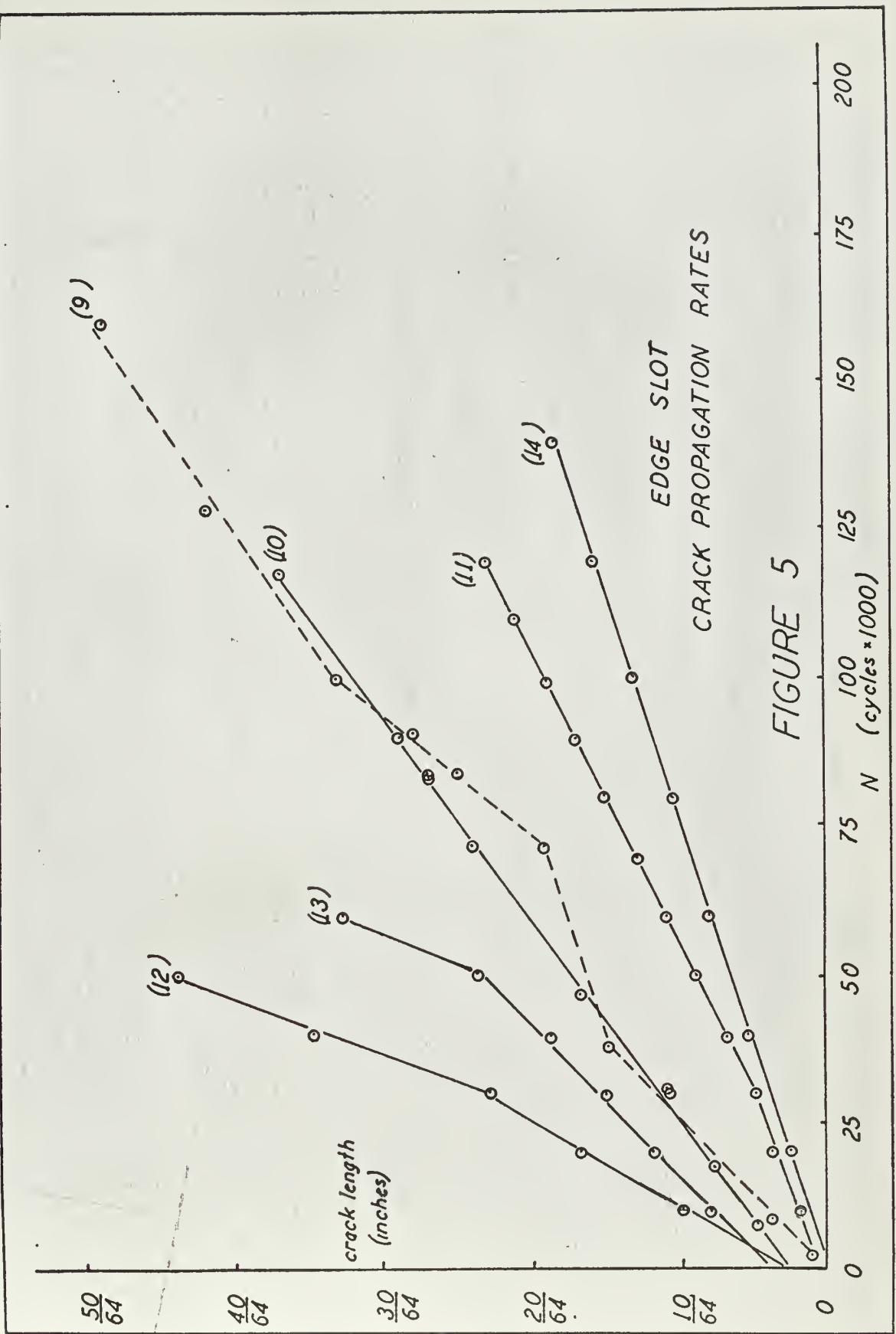
$$\text{STRESS} = \epsilon \times 10.5 \text{ (psi)}$$

FIGURE 3













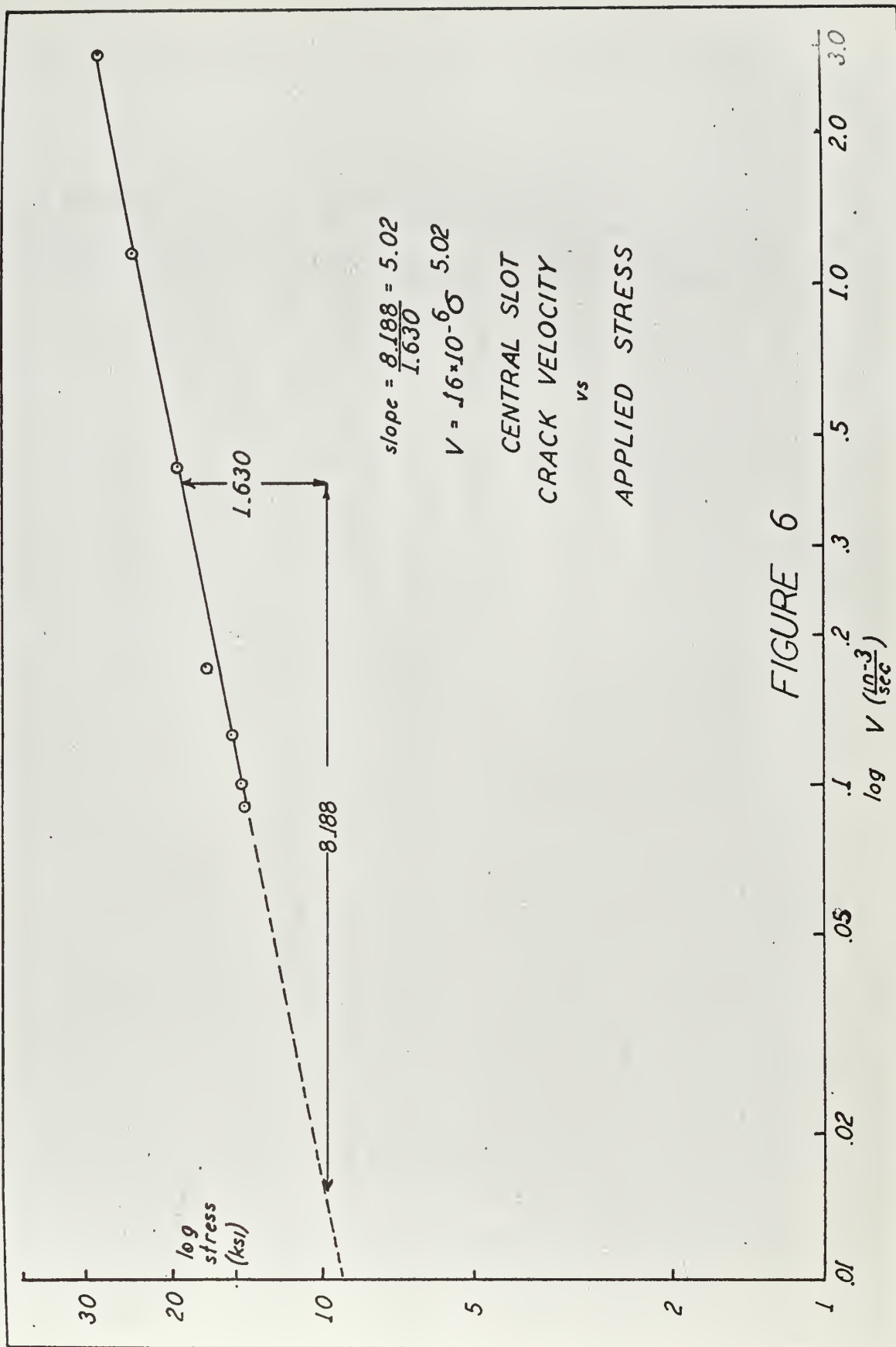


FIGURE 6



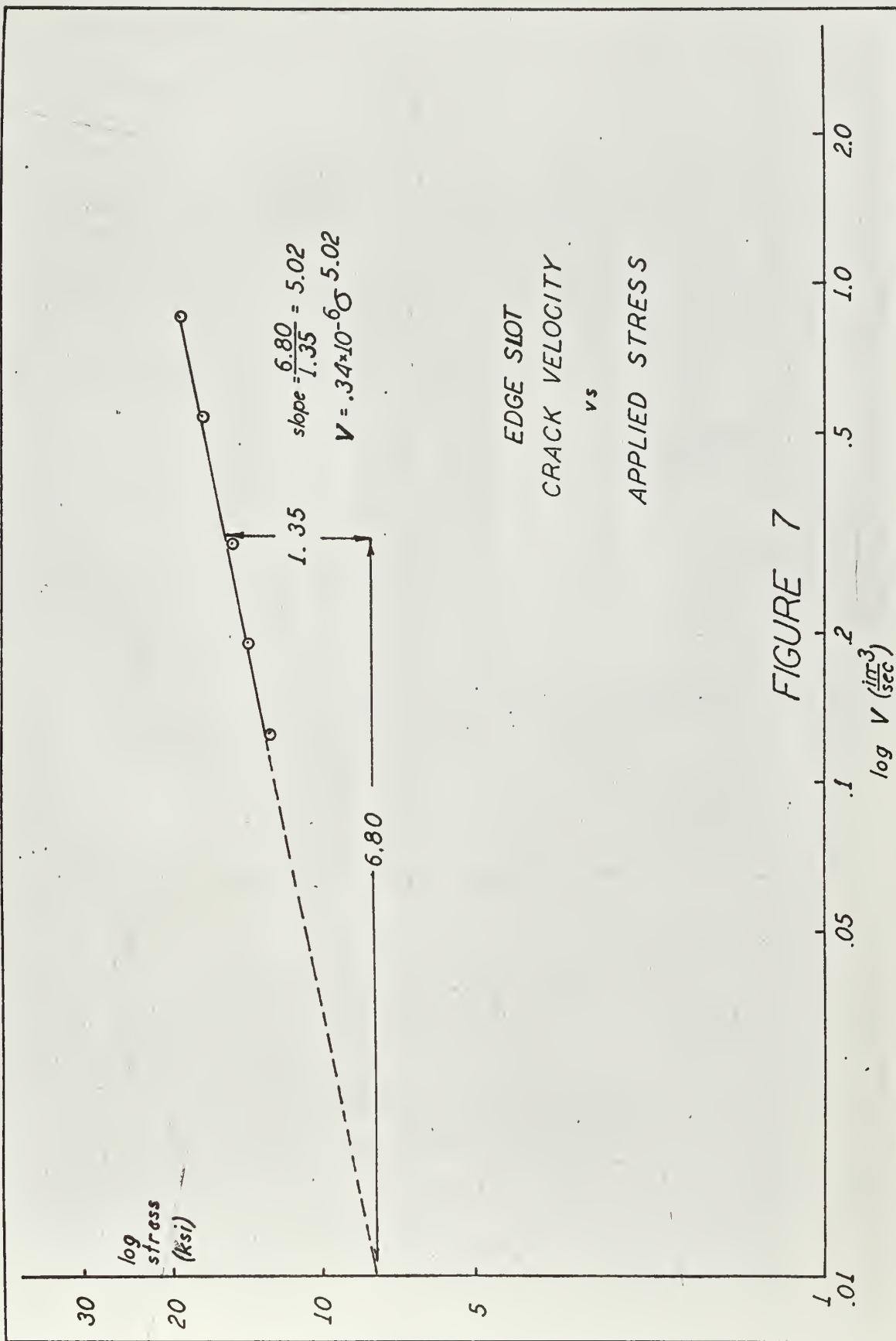
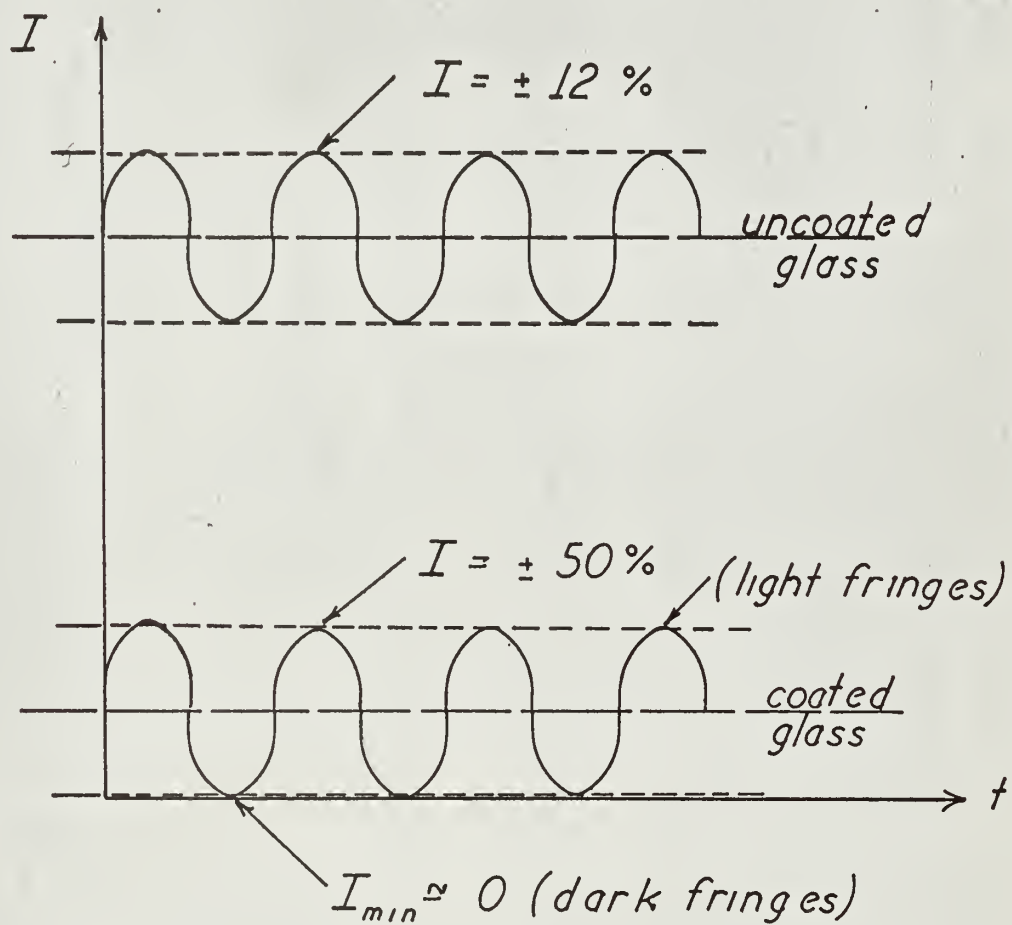


FIGURE 7



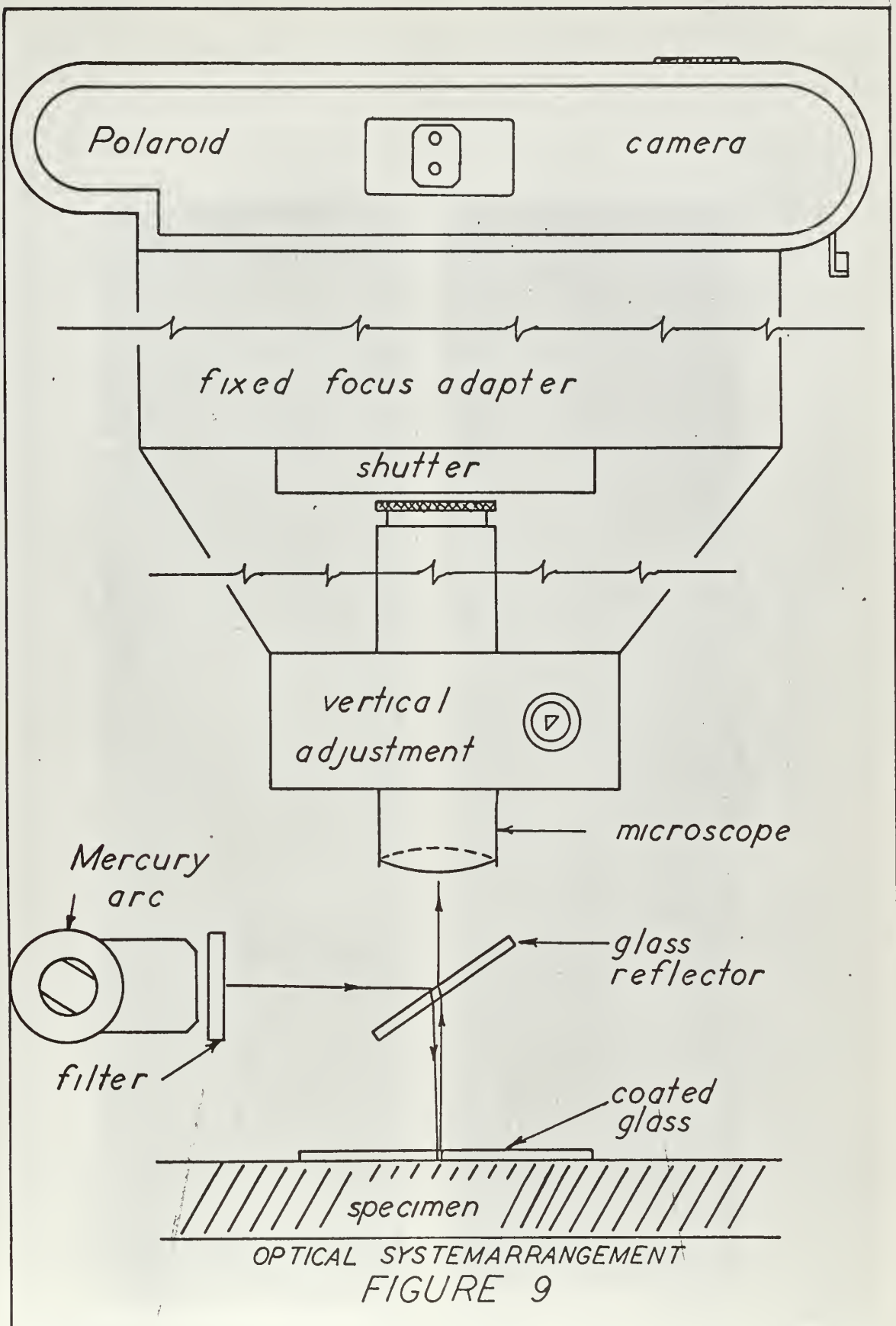




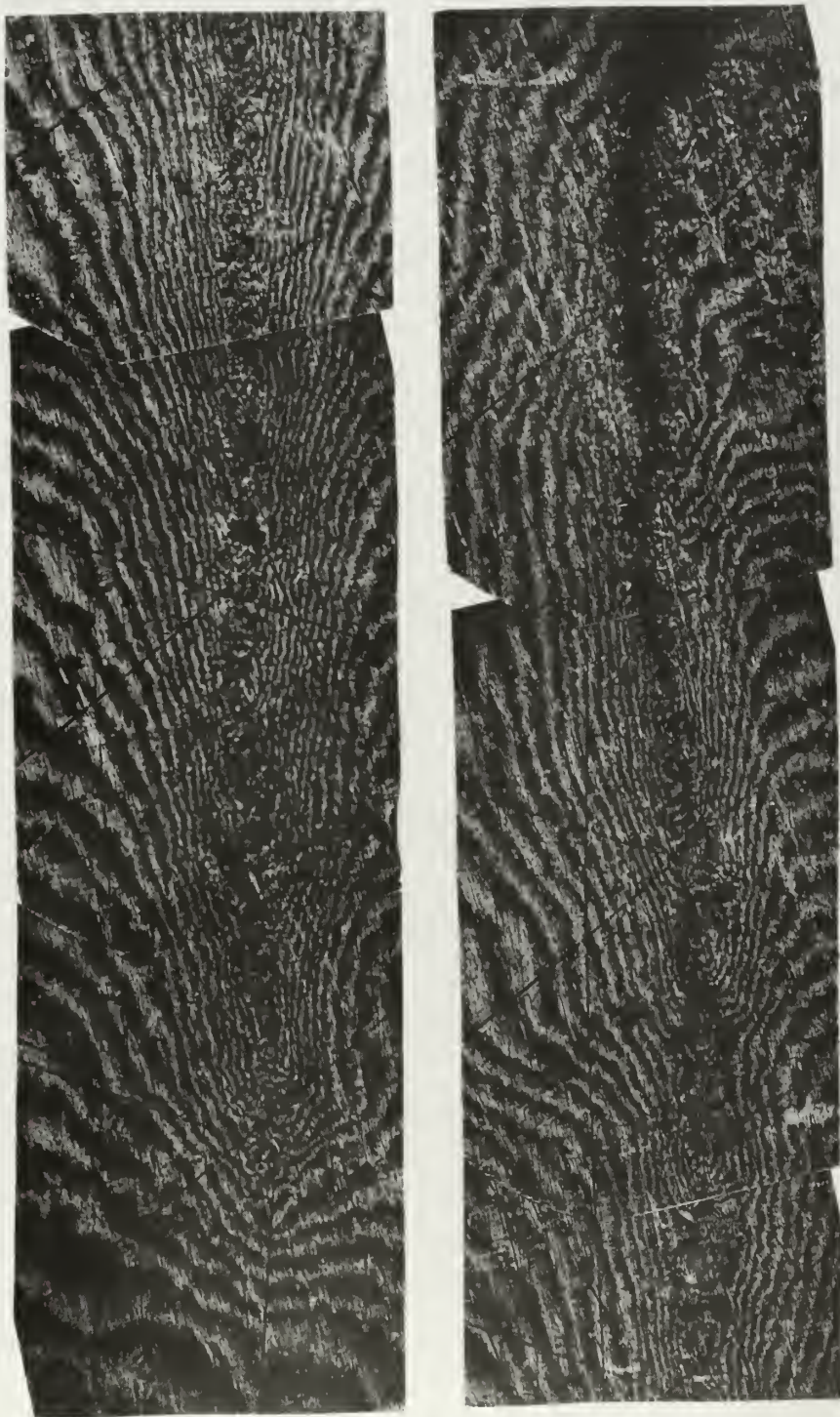
INTERFERENCE FRINGE INTENSITY  
WITH COATED AND UNCOATED COVER GLASS

FIGURE 8







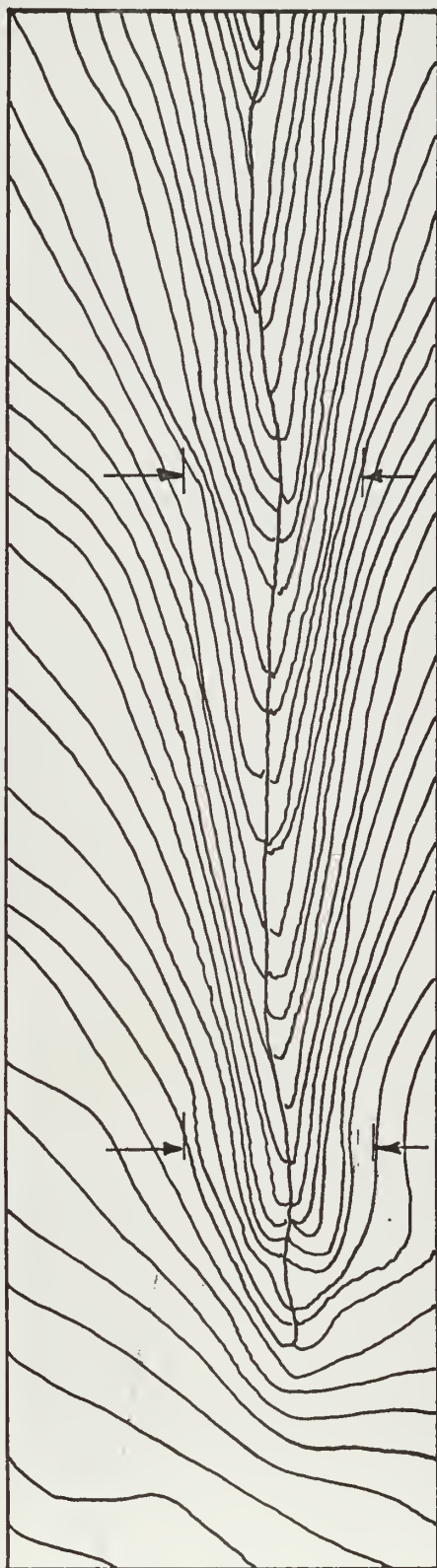


FRINGE PATTERN AROUND A CRACK

FIGURE 10







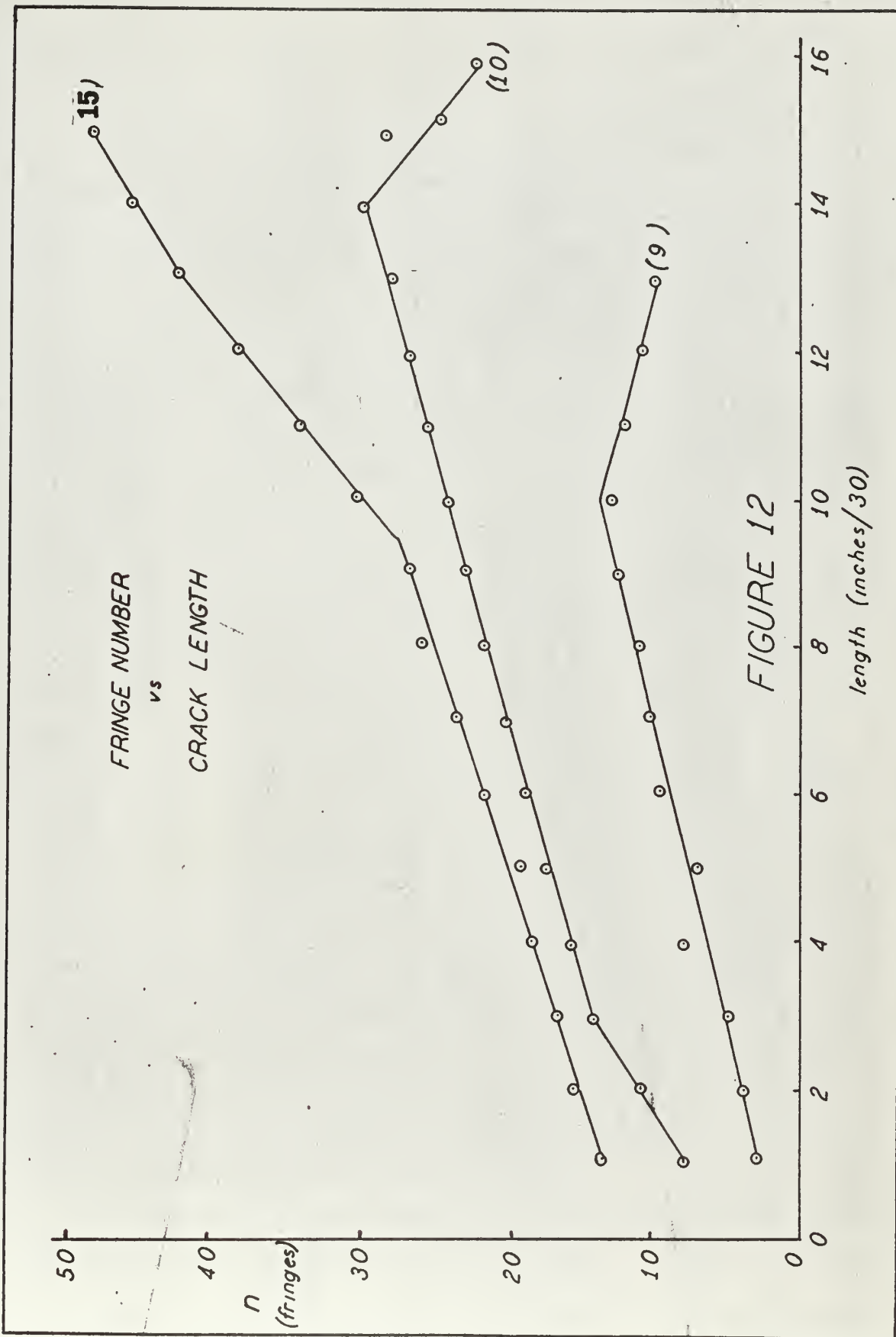
magnification —30

DEPRESSION WIDTH



FIGURE 11









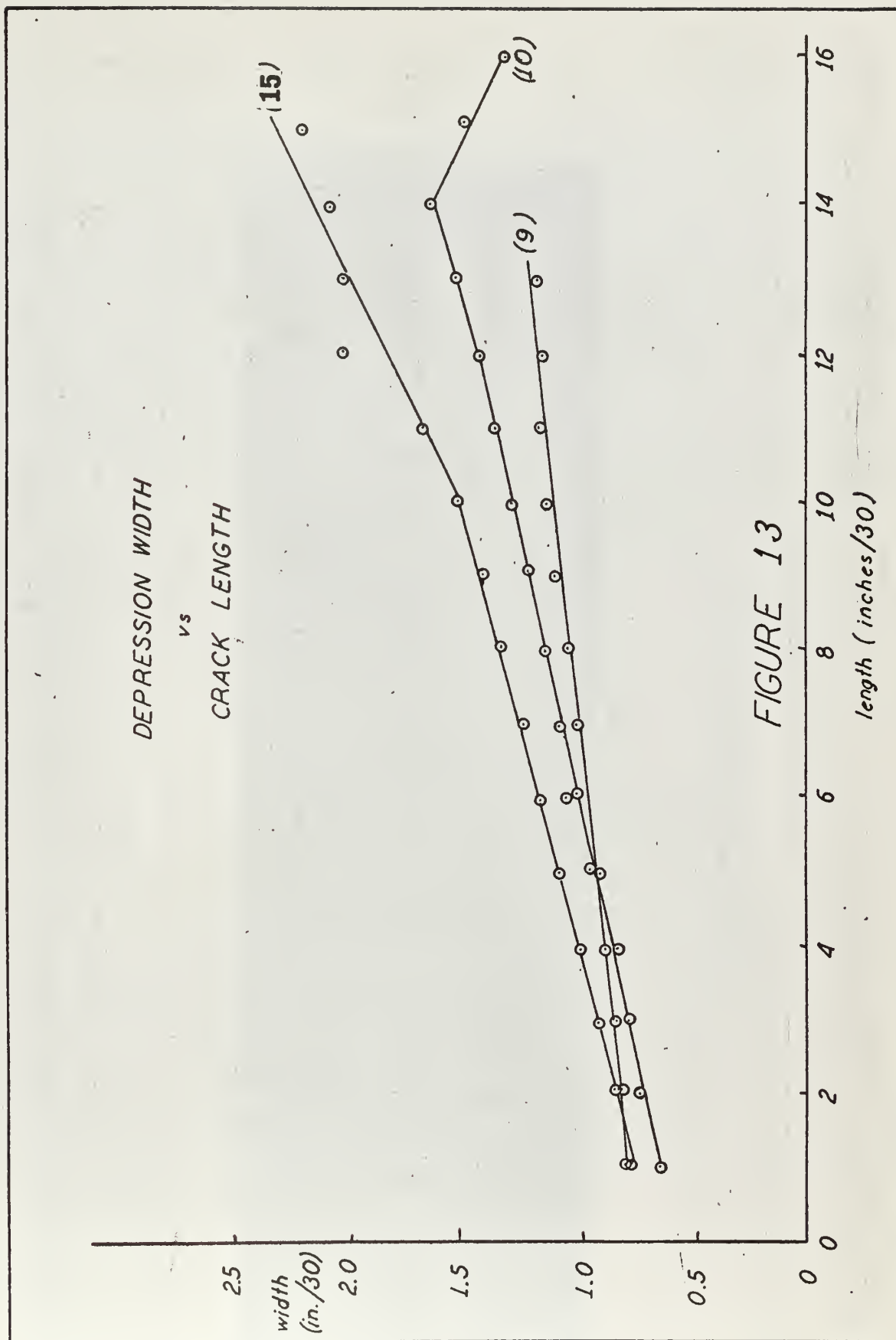
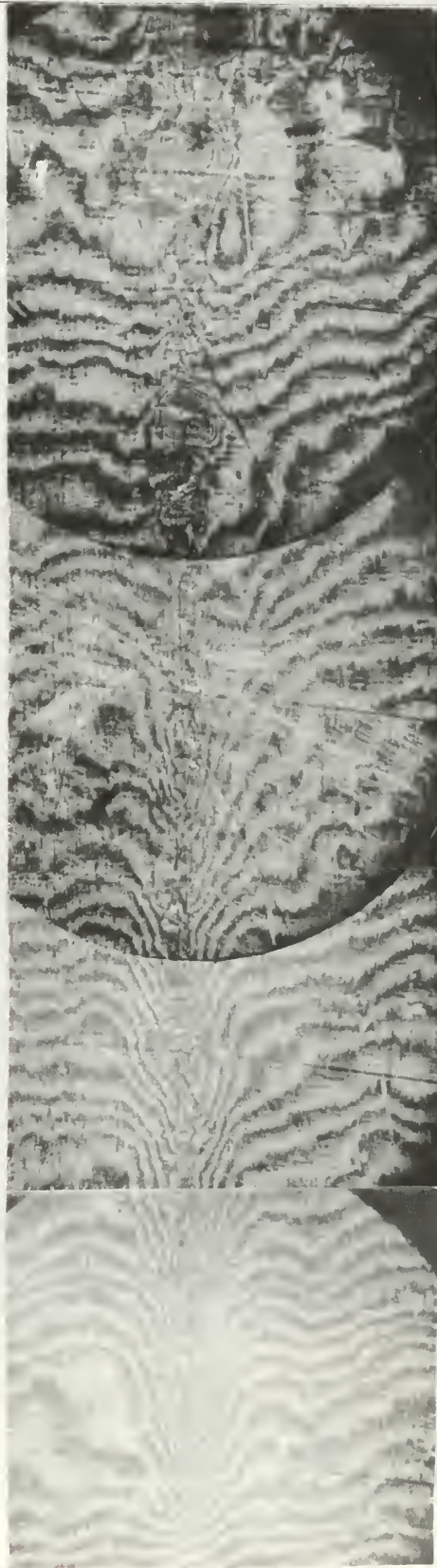


FIGURE 13





*CONCENTRIC FRINGE CONTOURS*

*FIGURE 14*



*METAL SURFACE SHOWING  
SLIP FORMATION*

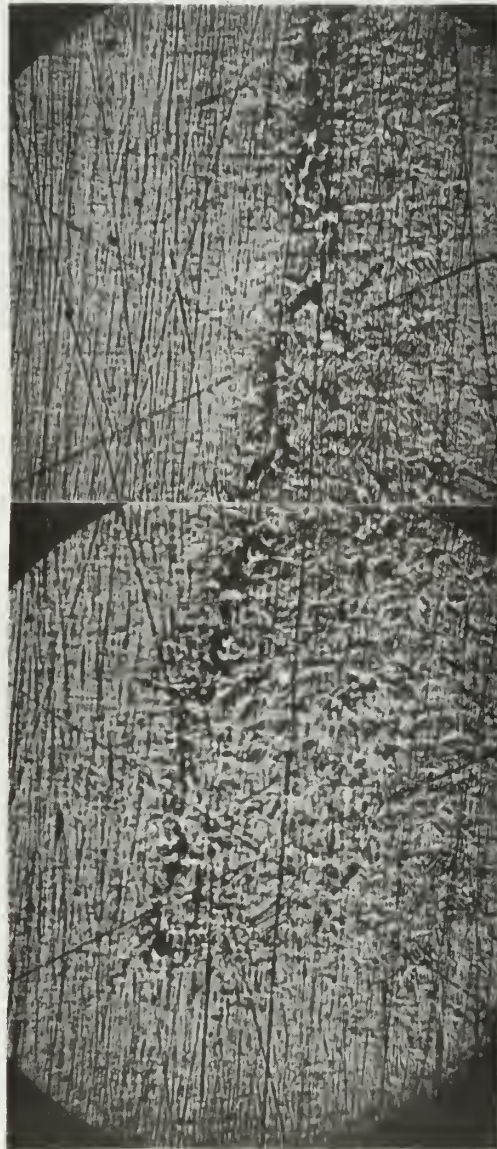
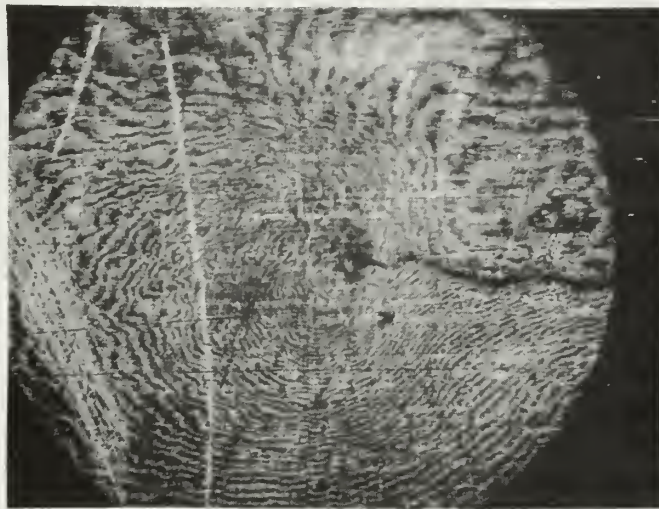


*FIGURE 15*

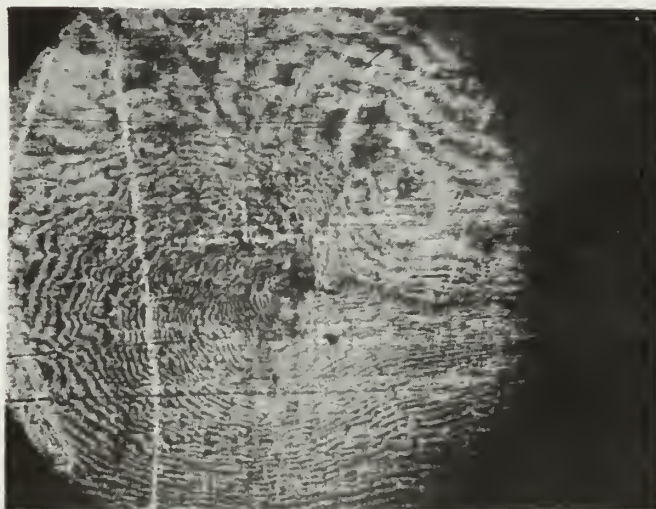






*2000 pound load*

*STRAIN CONTOURS UNDER  
TENSION*



*no load*

*FIGURE 16*



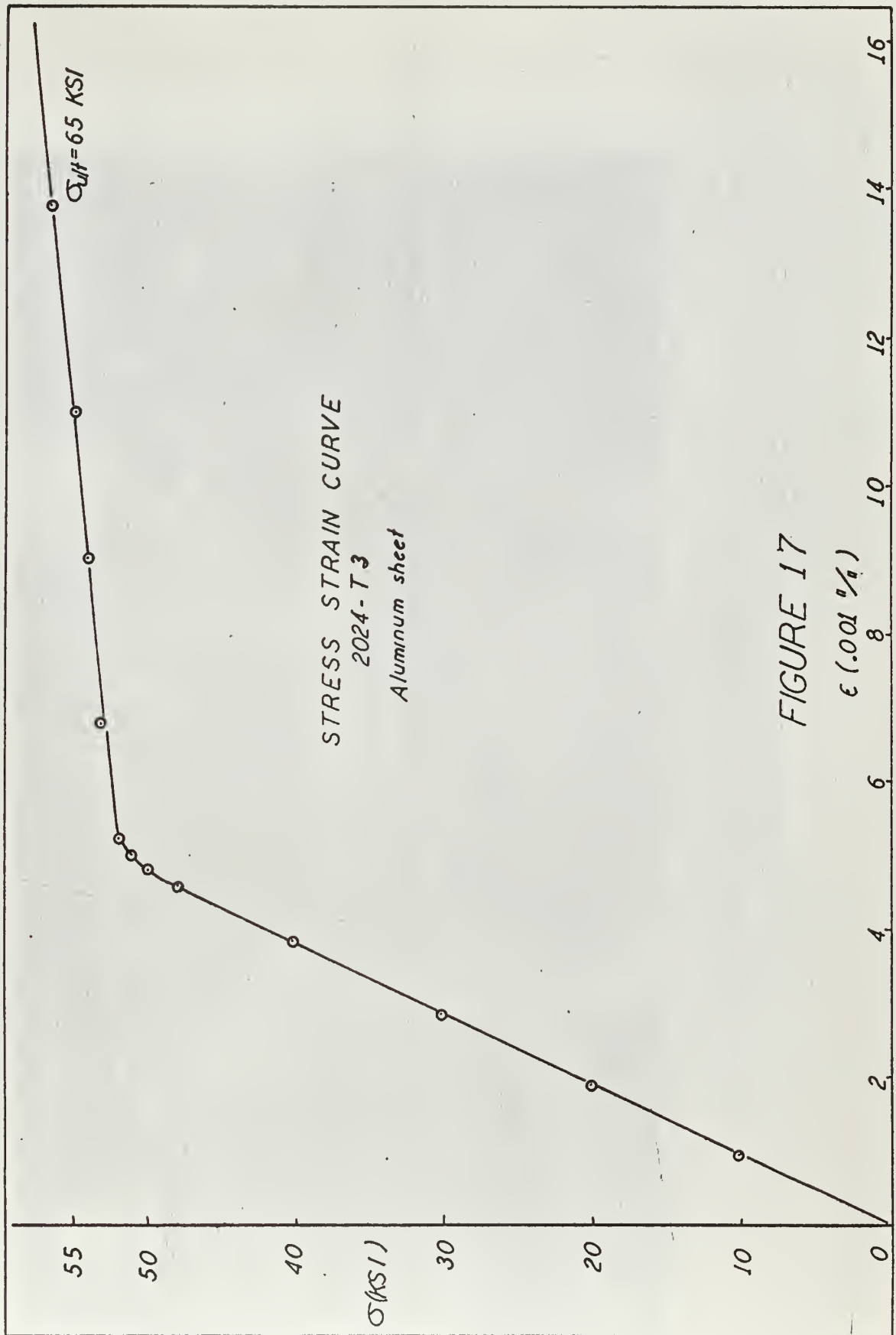


FIGURE 17



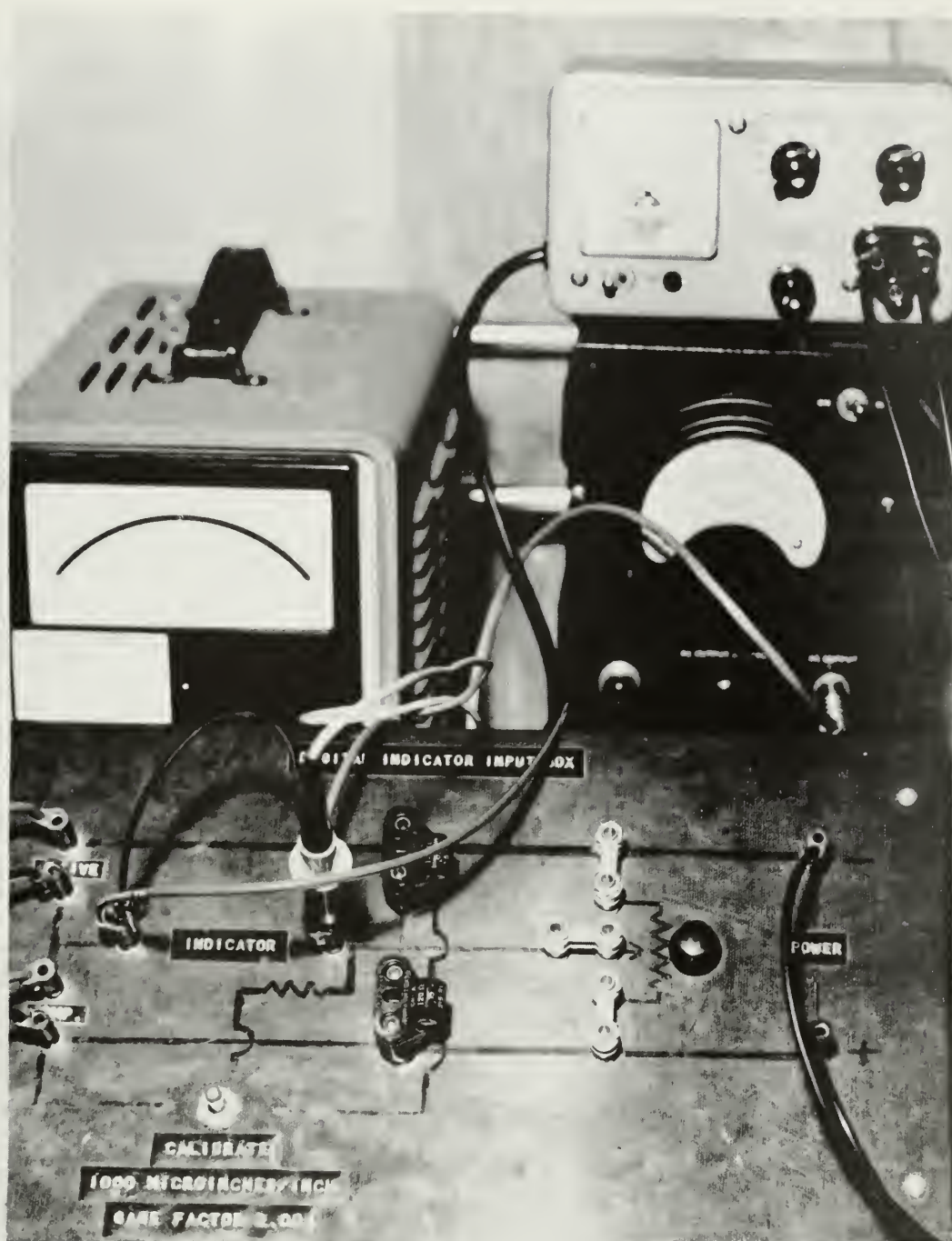


CALIDYNE SHAKER TABLE EQUIPMENT

FIGURE E-1



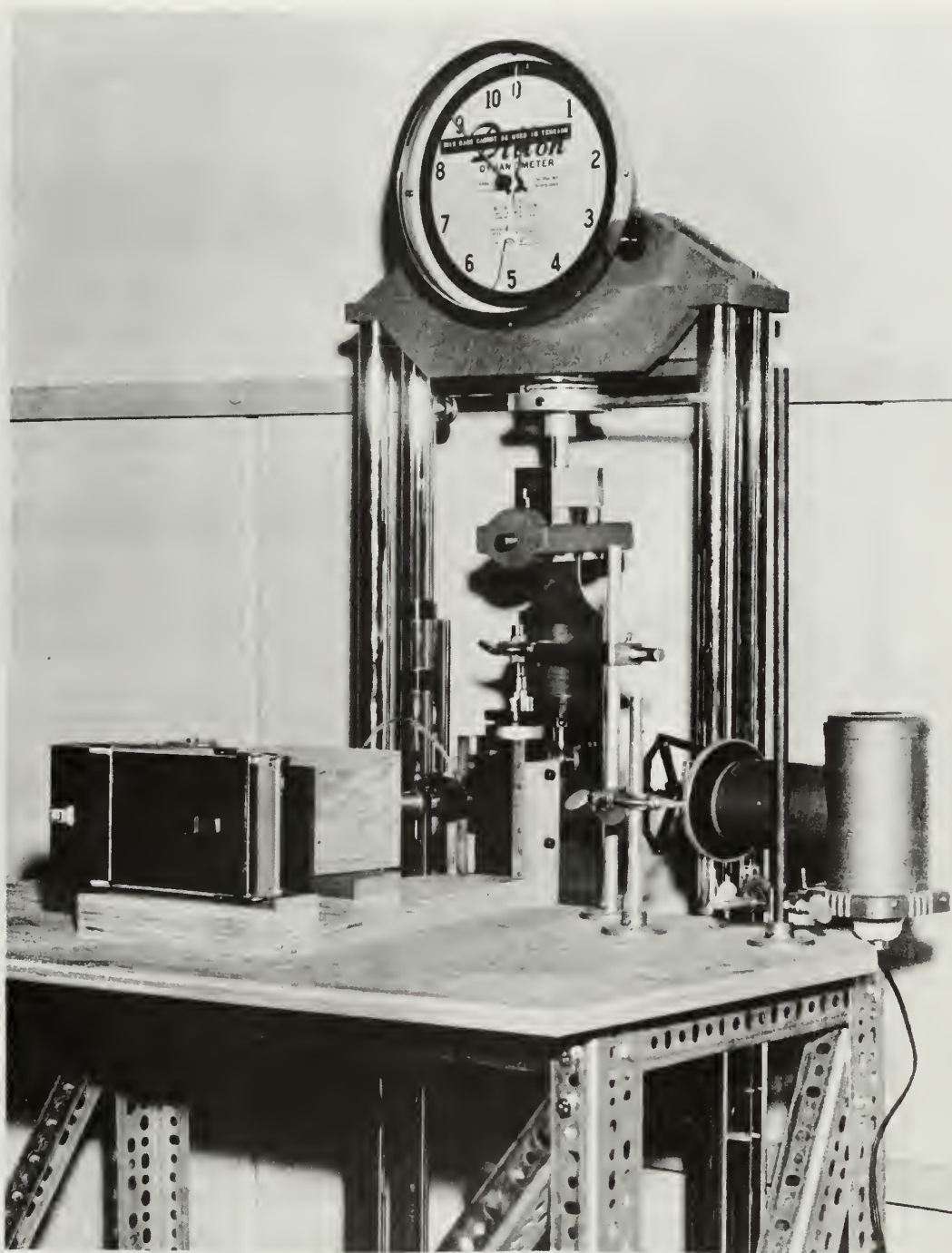




STRAIN GAGE MEASURING EQUIPMENT

FIGURE E-2

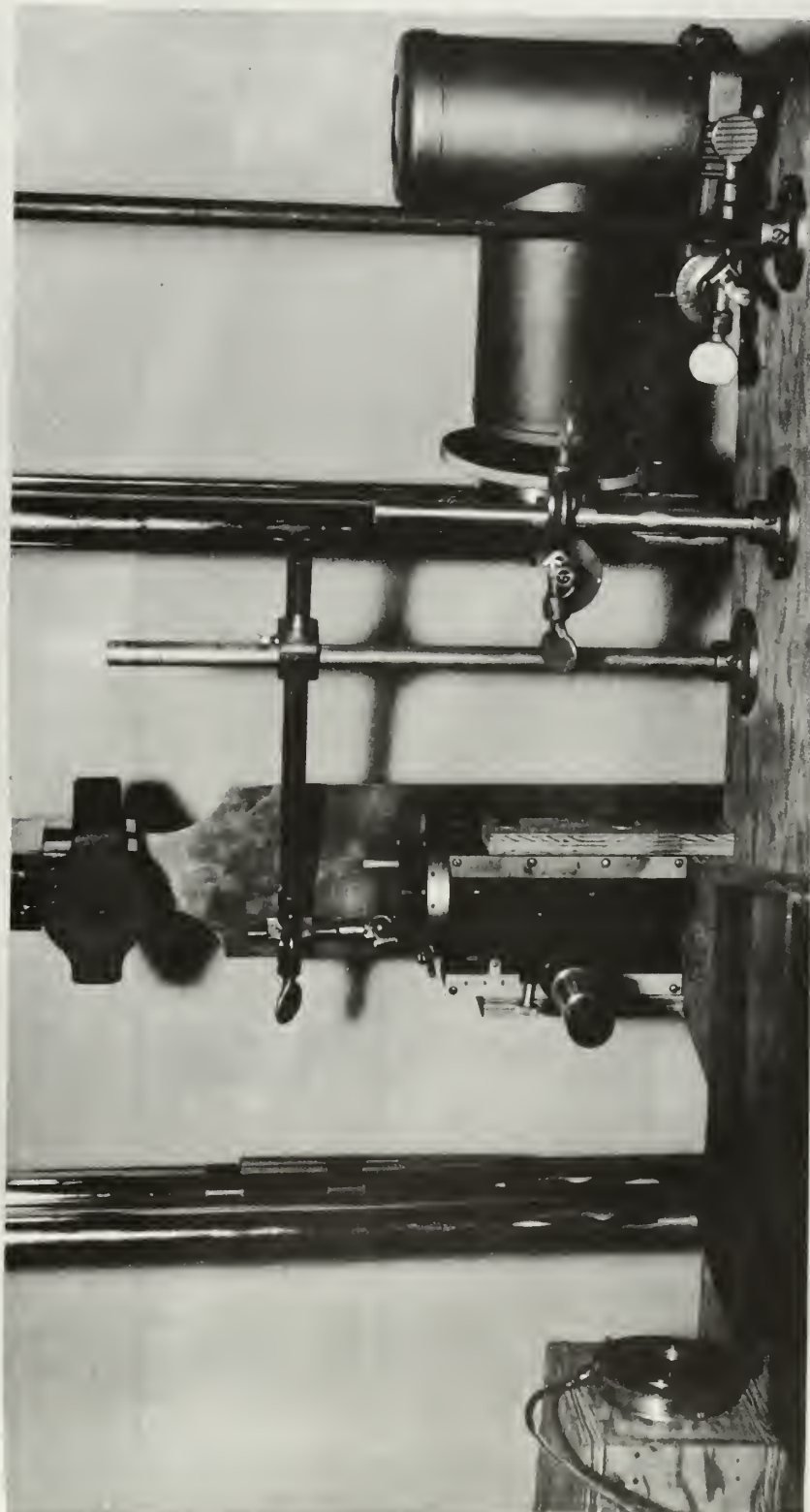




DILLON TESTING MACHINE ARRANGEMENT

FIGURE E-3





OPTICAL EQUIPMENT ARRANGEMENT

FIGURE E-4







TABLE I  
CRACK FATIGUE DATA

Specimen	Slot	Stress (KSI)	L (64ths)	N (Kc)
1	.757 x .012 central	15.85	1 24	5.823 200.079
2	.792 x .012 central	14.6	1 3 5 7 9 11 13 15 17	1.560 25.062 50.018 75.024 100.023 125.000 150.006 175.000 200.006
3	.738 x .012 central	14.6	.5 3 5 7 9 11 13 15 18	1.774 25.042 50.009 75.049 100.000 125.105 150.070 175.002 200.000
4	.757 x .012 central	19.5	1 8.5 15 26 36	1.500 20.007 40.003 60.001 80.000
5	.756 x .012 central	17.1	1 5 9 12 15 18	2.900 20.016 40.013 60.016 80.013 100.016
6	.744 x .012	29.3	16 23 26 53 one edge failure	5.006 10.010 15.019 20.000 21.369 30.000



TABLE I con't.

7	.730 x .008 central	15.85	1	21.207
			4	38.135
			4	45.608
			7	65.728
			10	103.890
			17	141.862
			21	165.637
8	.750 x .008 central	14.6	1	6.372
			1	12.791
			4	17.014
			8	49.200
			10	78.268
			12	102.086
			14	131.598
			16	151.464
			18	168.338
			20	189.239
			22	200.000
9	.797 x .012 edge	14.6	1	4.100
			4	8.449
			8	17.709
			11	31.020
			15	38.425
			19	72.387
			25	84.086
			28	91.781
			33	101.454
			42	128.131
10	.750 x .012 edge	14.6	49	160.070
			1	2.455
			5	8.513
			8	17.787
			11	31.267
			17	48.439
			24	72.382
			27	84.070
			29	91.843
			33	101.450
11	.746 x .012 edge	14.6	37	118.048
			1	1.328
			2	10.000
			4	20.001
			5	30.002
			7	40.007
			9	50.004
			11	60.004
			13	70.003



TABLE I con't.

12	.750 x .012 edge	19.5	15	80.000
			17	90.000
			19	100.004
			21	110.007
			23	120.012
13	.753 x .012 edge	17.1	1	1.500
			10	10.306
			17	20.002
			23	30.012
			35	40.000
14	.758 x .012 edge	12.2	44	50.003
			1	1.500
			8	10.002
			12	20.004
			15	30.006
15	.753 x .012 central	24.4	19	40.007
			23.5	50.006
			33	60.000
			0	2.290
			2.5	20.000
			5.5	40.011
			8	60.000
			10.5	80.000
			13	100.000
			16	120.000
			18.5	140.001
			20.5	160.000
			1	1.370
			6	5.000
			12	10.012
			18	15.013
			24	20.013
			32	25.016





TABLE II  
CRACK PROPAGATION RATES

Specimen	Stress	Propagation Rate	
		(10 <sup>-3</sup> ) in./sec.	in./cyc.
1	15.85	.127	2.02
2	14.60	.090	1.43
3	14.60	.090	1.43
4	19.50	.437	6.93
5	17.10	.180	2.86
6	29.20	2.70	42.90
7	15.85	.127	2.02
8	14.60	.100	1.59
9	14.60	.302	4.80
10	14.60	.308	4.88
11	14.60	.189	3.00
12	19.50	.867	13.80
13	17.10	.542	8.60
14	12.20	.126	2.00
15	24.40	1.28	20.30



TABLE III

STRAIN DISTRIBUTION DATA  
 AROUND A CIRCULAR HOLE  
 IN A FINITE SHEET

Specimen	Number of Fringes							
	0°	30°	90°	150°	180°	210°	270°	310°
A-1	1	0+	3-	0	1	0-	3	0
A-2	1	0	3	0	1	0	3	0
A-3	1	0	3	0	1	0	3	0
A-4	1	0	3	0	1-	0	3	0
A-5	1-	0-	3+	0	1	0+	3	0+
A-6	1	0	3	0	1	0	3	0



TABLE IV  
CRACK DEPRESSION GEOMETRY

Specimen	L (in./30)	W (in./30)	n
9 14.6 KSI	1	5/8	3
	2	3/4	3
	3	13/16	5
	4	15/16	9
	5	7/8	6
	6	1 1/16	10
	7	1	10
	8	1	10
	9	1 1/8	12
	10	1 1/8	12
	11	1 1/8	12
	12	1 1/16	10
	13	1 1/8	10
10 14.6 KSI	1	5/8	8
	2	11/16	9
	3	3/4	14
	4	11/16	15
	5	1	17
	6	1	19
	7	1 1/16	20
	8	1 1/8	22
	9	1 3/16	22
	10	1 1/4	24
	11	1 5/16	25
	12	1 3/8	25
	13	1 1/2	25
	14	1 5/8	30
	15	1 1/2	28
	16	1 1/4	22
15 24.4 KSI	1	3/4	14
	2	13/16	16
	3	7/8	16
	4	1	18
	5	1 1/16	18
	6	1 1/8	20
	7	1 3/16	24
	8	1 1/4	27
	9	1 3/8	26
	10	1 1/2	30
	11	1 5/8	34
	12	2	38
	13	2	43
	14	2	45
	15	2 1/8	47





TABLE V  
GEOMETRY OF CONCENTRIC FRINGE PATTERNS

Specimen	L (in./30)	Dia. (in./30)	n
7 15.85 KSI	3/4	5/8	10
	2 3/8	3/8	13
	2 15/16	1/4	5
	6 1/2	3/16	3
	7 1/2	5/32	3
	8 1/2	5/8	4
8 14.60 KSI	5/32	1/4	7
	25/32	1/8	4
	1 1/2	3/8	12
	2 5/8	3/32	3
	3	3/32	4
	3 1/2	3/8	7
	4 5/16	5/32	5
9 14.60 KSI	2 1/2	1/3	3
	2 31/32	1/8	5
	4 3/8	3/8	4
	5 1/2	9/16	7
	6 5/8	1/4	5
	8 25/32	5/32	4
	9 3/8	1/4	6
	9 11/16	5/32	6



## APPENDIX 1

### DETERMINATION OF STRAINS FROM INTERFEROMETRIC FRINGE PATTERNS

#### 1. For the Elastic Range [24]

$$\epsilon_1 = \frac{1}{E} (\sigma_1 - \nu \sigma_2) \quad \sigma_1 + \sigma_2 = \frac{E}{1-\nu} (\epsilon_1 + \epsilon_2)$$

$$\epsilon_2 = \frac{1}{E} (\sigma_2 - \nu \sigma_1)$$

$$\epsilon_3 = -\frac{\nu}{E} (\sigma_1 + \sigma_2)$$

$$\epsilon_3 = -\frac{\nu}{1-\nu} (\epsilon_1 + \epsilon_2)$$

At a free boundary  $\sigma_2 = 0$

$$\epsilon_1 = \frac{\sigma_1}{E}$$

$$\epsilon_2 = -\frac{\nu}{E} \sigma_1 \quad \epsilon_2 = \epsilon_3 = -\nu \epsilon_1$$

$$\epsilon_3 = -\frac{\nu}{E} \sigma_1$$

#### 2. For the Plastic Range

$$\epsilon_1 + \epsilon_2 + \epsilon_3 = 0 \quad \epsilon_3 = -(\epsilon_1 + \epsilon_2)$$

At a free boundary

$$\epsilon_2 = \epsilon_3 = -\frac{1}{2} \epsilon_1$$

#### 3. Relation of $\epsilon_3$ to Interference Lines

$$\frac{n\lambda}{2} = \mu t \cos \theta \quad [25, 26, 27]$$

$$\cos \theta = 1$$

$$\mu = 1$$

$$\lambda = 5460.74 \text{ \AA}$$

$$t = \frac{n\lambda}{2} \quad \text{or} \quad n\lambda = 2t$$

$$\Delta z = 2t$$

$$z = .0625 \text{ in}$$

$$\epsilon_3 = \frac{\Delta z}{z} = \frac{n\lambda}{z}$$

$$\epsilon_3 = \left( \frac{5460.74}{25.4} \right) \left( \frac{10^{-3}}{.0625} \right)$$

$$\epsilon_3 = 348 \times 10^{-6} \text{ in/in per fringe}$$



## APPENDIX 2

### REVERSE BENDING CALCULATIONS

For harmonic vibration of a beam of constant cross section,

$$EI \frac{d^4 w}{dx^4} - \rho \omega^2 w = 0$$

$$\text{let } \beta^4 = \rho \omega^2 / EI$$

$$\text{then } \frac{d^4 w}{dx^4} - \beta^4 w = 0 \quad \text{characteristic equation } \lambda^4 - \beta^4 = 0$$

$$\lambda = \beta \sqrt[4]{1}$$

$$W = A \cosh \beta x + B \sinh \beta x + C \cos \beta x + D \sin \beta x$$

For a cantilever beam of length  $l$  clamped at  $x=0$ ,

$$W|_0 = 0 \quad \frac{dW}{dx}|_0 = 0 \quad \frac{d^2 W}{dx^2}|_l = 0 \quad \frac{d^3 W}{dx^3}|_l = 0$$

$$\therefore (A+C) + (B+D) = 0$$

$$W = A (\cosh \beta l - \cos \beta l) + B (\sinh \beta l - \sin \beta l)$$

$$\rho = .649 \times 10^{-4} \frac{\text{slugs}}{\text{in}} \quad I = 81.38 \times 10^{-6} \text{ in.}^4 \quad E = 10.6 \times 10^6 \text{ psi}$$

$$\text{for second mode } \omega = (1.49)^2 \frac{\pi^2}{l^2} \sqrt{\frac{EI}{\rho}}, \quad \sqrt{\frac{EI}{\rho}} = 3654.4$$

$$\frac{(1.49)^2 \pi^2}{(15)^2} = .09737 \quad \omega = 355.841 \text{ rad/sec} \quad f = 56.634 \text{ cyc/sec.}$$

Equivalent length due to end cut out 14.2 inches.

$$f_{\text{equiv}} = 63 \text{ cyc/sec.}$$

$$\beta^4 = \frac{\omega^2 \rho}{EI} = .009482 \quad \beta^2 = .09738 \quad \beta = .31205$$

$$\beta l = 4.6807 = 268^\circ 10' 48''$$

$$\sinh \beta l \quad 53.95924 \quad \sin \beta l \quad -.99950$$

$$\cosh \beta l \quad 53.96853 \quad \cos \beta l \quad -.03170$$

$$W'' = A (\cosh \beta l + \cos \beta l) + B (\sinh \beta l + \sin \beta l) = 0$$

$$\frac{A}{B} = - \left( \frac{\sinh \beta l + \sin \beta l}{\cosh \beta l + \cos \beta l} \right) = - \frac{52.95974}{53.93683} = -.98188$$

$$W = A [\cosh \beta x - \cos \beta x - .98188 (\sinh \beta x - \sin \beta x)]$$





for  $W_{\max}$ ,  $W' = 0$

$$W' = .31205 A [\sinh \beta x + \sin \beta x - .98188 (\cosh \beta x - \cos \beta x)] = 0$$

$$\frac{\sinh \beta x + \sin \beta x}{\cosh \beta x - \cos \beta x} = .98188 \text{ for } W_{\max}$$

$$\text{let } \beta x = 2.361 = 135^{\circ} 16' 31''$$

$$\sinh \beta x = 5.25350 \quad \cosh \beta x = 5.34760$$

$$\sin \beta x = .69810 \quad \cos \beta x = -.71600$$

$$\frac{5.95160}{6.06360} = .98153$$

$$X_{\max} = \frac{2.361}{.31205} = 7.566 \text{ in.} \quad X_{\max(\text{eff})} = 7.566 \left( \frac{56.6}{63} \right) = 6.72 \text{ in.}$$

$$M = EI W'' \quad \sigma = \frac{M Y}{I} = E Y W''$$

$$\sigma = (10.6)(.03125) 10^6 W'' = 33.125 \times 10^4 W''$$

$$W'' = A(.09738) [\cosh 2.361 + \cos 2.361 - .98153 (\sinh 2.361 + \sin 2.361)]$$

$$\sigma = 39,033 A \text{ psi}$$

let  $A$  = Amplitude in inches

$$\underline{\underline{\sigma = 39,033 \text{ psi per inch deflection}}}$$

$$\sigma_{\frac{3}{4}} = 29,274 \text{ psi}$$

$$\sigma_{\frac{1}{2}} = 19,516 \text{ psi}$$

$$\sigma_{\frac{13}{32}} = 15,850 \text{ psi}$$

$$\sigma_{\frac{3}{8}} = 14,637 \text{ psi}$$

$$\sigma_{\frac{1}{4}} = 9,758 \text{ psi}$$



## Strain gage calibration of bending calculations

For 1/4 inch amplitude

$$\text{Meter output} = 1.90 \text{ mV(rms)} = 2.68 \text{ mV Peak}$$

$$\text{Meter sensitivity} = \frac{3 \text{ mV}}{1000 \mu\text{"/"}}$$

$$\text{Strain} = (2.68) (1000/3) = 995 \mu\text{"/"}$$

$$\text{Stress} = E \epsilon = (995) (10.6) = 9480 \text{ psi}$$

$$\text{Stress calculated} = 9758 \text{ psi}$$

$$\% \text{ difference} = \frac{(278) (100)}{(9758)} = 2.85\%$$

For 3/8 inch amplitude

$$\text{Meter output} = 2.85 \text{ mV(rms)} = 4.03 \text{ mV Peak}$$

$$\text{Meter sensitivity} = \frac{3 \text{ mV}}{1000 \mu\text{"/"}}$$

$$\text{Strain} = (4.03) \left( \frac{1000}{3} \right) = 1341 \mu\text{"/"}$$

$$\text{Stress} = (10.6) (1341) = 14,100 \text{ psi}$$

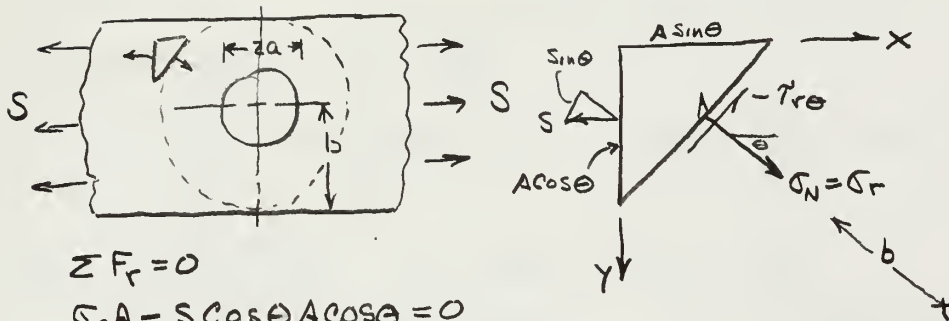
$$\text{Stress calculated} = 14,637 \text{ psi}$$

$$\% \text{ difference} = \frac{(537) (100)}{(14637)} = 3.67\%$$



### APPENDIX 3

#### DEVELOPMENT OF STRESS DISTRIBUTION AROUND A CIRCULAR HOLE IN A THIN INFINITE PLATE



$$\sum F_r = 0$$

$$\sigma_r A - S \cos \theta A \cos \theta = 0$$

$$\sigma_r = S \cos^2 \theta = \frac{S}{2} (1 + \cos 2\theta)$$

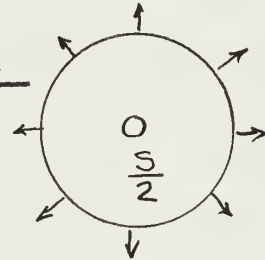
$$\sum F_\theta = 0$$

$$-\tau_{r\theta} A - S \sin \theta A \cos \theta = 0 \quad \tau_{r\theta} = -\frac{S}{2} \sin 2\theta$$

PART I

$$\sigma_r = \frac{S}{2}$$

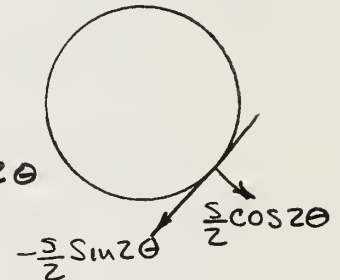
$$\tau_{r\theta} = 0$$



PART II

$$\sigma_r = \frac{S}{2} \cos 2\theta$$

$$\tau_{r\theta} = -\frac{S}{2} \sin 2\theta$$



PART I  $\sigma_r|_{r=a} = 0 \quad \sigma_r|_{r \rightarrow \infty} = \frac{S}{2} \quad S_\theta = 0$

$$\nabla^4 \phi = \frac{d^4 \phi}{dr^4} + \frac{2}{r} \frac{d^3 \phi}{dr^3} - \frac{1}{r^2} \frac{d^2 \phi}{dr^2} + \frac{1}{r^3} \frac{d\phi}{dr} = 0$$

$$\tau_{r\theta} = 0 \quad \sigma_r = \frac{1}{r} \frac{\partial \phi}{\partial r} \quad \sigma_\theta = \frac{\partial^2 \phi}{\partial r^2}$$

let  $r = e^t$   $dr = e^t dt$   $\frac{dt}{dr} = e^{-t}$   $\frac{d\phi}{dr} = \frac{\partial \phi}{\partial t} \frac{dt}{dr} = e^{-t} \frac{d\phi}{dt}$

$$\frac{\partial^2 \phi}{\partial r^2} = \frac{d}{dt} \left[ e^{-t} \frac{d\phi}{dt} \right] e^{-t} = e^{-2t} \left[ \frac{\partial^2 \phi}{\partial t^2} - \frac{\partial \phi}{\partial t} \right]$$

$$D = \frac{d}{dt} \quad r \frac{d\phi}{dr} = D(\phi) \quad r^2 \frac{d^2 \phi}{dr^2} = D(D-1)\phi, \quad r^3 \frac{d^3 \phi}{dr^3} = D(D-1)(D-2)\phi$$

$$r^4 \nabla^4 \phi = r^4 \frac{d^4 \phi}{dr^4} + 2r^3 \frac{d^3 \phi}{dr^3} - r^2 \frac{d^2 \phi}{dr^2} + r \frac{d\phi}{dr} = 0$$

$$D^4 - 6D^3 + 4D^2 - 6D$$

$$2D^3 - 6D^2 + 4D$$

$$-D^2 + D$$

$$+D$$

$$[D^4 - 4D^3 + 4D^2] \phi = 0$$

then  $\frac{\partial^4 \phi}{\partial t^4} - 4 \frac{\partial^3 \phi}{\partial t^3} + 4 \frac{\partial^2 \phi}{\partial t^2} = 0$





$$\text{let } \varphi = e^{mt} \quad (m^4 - 4m^3 + 4m^2) e^{mt} = 0 \quad e^{mt} \neq 0$$

$$m^4 - 4m^3 + 4m^2 = 0 \quad m = 0, 0, 2, 2$$

$$\varphi = A e^{0t} + B t e^{0t} + C e^{2t} + D t e^{2t}$$

$$\text{let } \ln r = t \quad \varphi = A + B \ln r + C r^2 + D r^2 \ln r$$

$$\sigma_r = \frac{1}{r} \frac{\partial \varphi}{\partial r} \quad \sigma_\theta = \frac{\partial^2 \varphi}{\partial r^2}$$

$$\sigma_r = \frac{B}{r^2} + 2C + D(2 \ln r + 1) \quad \sigma_\theta = -\frac{B}{r^2} + 2C + D(2 \ln r + 3)$$

$$\tau_{r\theta} = 0$$

FOR DEFLECTIONS  $\epsilon_r = \frac{1}{E} (\sigma_r - \mu \sigma_\theta) = \frac{\partial u}{\partial r}$

$$\epsilon_\theta = \frac{1}{E} (\sigma_\theta - \mu \sigma_r) = \frac{u}{r} + \frac{1}{r} \frac{\partial r}{\partial \theta} \quad \gamma_{r\theta} = \frac{2(1+\mu)}{E} \tau_{r\theta} = \frac{1}{r} \frac{\partial u}{\partial \theta} + \frac{\partial r}{\partial \theta} - \frac{u}{r}$$

$$\frac{\partial u}{\partial r} = \frac{1}{E} \left[ \frac{(1+\mu)B}{r^2} + 2(1-\mu)D \ln r + (1-3\mu)D + 2(1-\mu)C \right]$$

$$\frac{u}{r} = -\frac{B}{Er^2} (1+\mu) + \frac{Dr(1-3\mu)}{rE} + \frac{2D(1-\mu)}{Er} (r \ln r - r) + \frac{2Cr(1-\mu)}{rE} + \frac{f(\theta)}{r}$$

$$\epsilon_\theta = \frac{1}{r} \frac{\partial r}{\partial \theta} + \frac{u}{r} = \frac{\sigma_\theta}{E} - \mu \frac{\sigma_r}{E} \quad \text{or} \quad \frac{1}{r} \frac{\partial r}{\partial \theta} = \frac{\sigma_\theta}{E} - \mu \frac{\sigma_r}{E} - \frac{u}{r}$$

$$\frac{1}{r} \frac{\partial r}{\partial \theta} = -\frac{B}{r^2} \frac{(1-\mu)}{E} + \frac{D(3-\mu)}{E} + \frac{2D(1-\mu)}{E} \ln r + \frac{2C(1-\mu)}{E} + \frac{B(1+\mu)}{r^2 E} - \frac{D}{E} (1-3\mu) + \frac{2D}{r} (1-\mu) - \frac{2D}{E} (1-\mu) \ln r + \frac{f(\theta)}{r} - \frac{2C(1-\mu)}{E}$$

$$\frac{1}{r} \frac{\partial r}{\partial \theta} = \frac{4D}{E} - \frac{f(\theta)}{r} \quad \frac{\partial r}{\partial \theta} = \frac{4Dr}{E} - f(\theta)$$

$$r = \frac{4Dr\theta}{E} - \int f(\theta) d\theta + f_1(r)$$

$$\gamma_{r\theta} \equiv 0, \quad \frac{1}{r} \frac{\partial f(\theta)}{\partial \theta} + \frac{4D\theta}{E} + \frac{\partial f_1(r)}{\partial r} - \frac{4D\theta}{E} + \frac{1}{r} \left[ \int f(\theta) d\theta - \frac{f_1(r)}{r} \right] \equiv 0$$

$$\frac{1}{r} \left[ \frac{\partial f(\theta)}{\partial \theta} + \int f(\theta) d\theta \right] + \left[ \frac{\partial f_1(r)}{\partial r} - \frac{f_1(r)}{r} \right] \equiv 0$$

$$\text{BOTH BRACKETS MUST} = 0 \quad \therefore \frac{\partial f_1(r)}{f_1(r)} = \frac{dr}{r}$$

$$\ln f_1(r) = \ln r + \ln c, \quad f_1(r) = F(r)$$

$$f(\theta) = -\frac{\partial}{\partial \theta} \left[ \frac{\partial f(\theta)}{\partial \theta} \right] = H \sin \theta + K \cos \theta$$

$$r = \frac{4Dr\theta}{E} + F(r) + H \cos \theta + K \sin \theta$$

for  $r$  to be single valued,  $D=0$

$$\sigma_r = \frac{B}{r^2} + 2C \quad \sigma_\theta = -\frac{B}{r^2} + 2C$$



### BOUNDARY CONDITIONS

$$\sigma_r|_{r=a} = -p_i \quad \sigma_r|_{r=b} = -p_o$$

$$\sigma_{ra} = \frac{B}{a^2} + 2C = -p_i$$

$$B + 2Ca^2 + p_i a^2 = 0$$

$$\sigma_{rb} = \frac{B}{b^2} + 2C = -p_o$$

$$B + 2Cb^2 + p_o b^2 = 0$$

$$B = \frac{a^2(p_o b^2 - p_i a^2)}{(b^2 - a^2)} - p_i a^2$$

$$2B + 2C(a^2 + b^2) + p_i a^2 + p_o b^2 = 0$$

$$2C(a^2 - b^2) + p_i a^2 - p_o b^2 = 0$$

$$2C = \frac{p_o b^2 - p_i a^2}{a^2 - b^2}$$

$$B = \frac{a^2 b^2 (p_o - p_i) - p_i a^4 + p_o a^4}{(b^2 - a^2)}$$

$$\sigma_r = \frac{1}{r^2} \frac{a^2 b^2 (p_o - p_i)}{b^2 - a^2} + \frac{p_i a^2 - p_o b^2}{b^2 - a^2} \quad \text{but } p_i = 0$$

$$\sigma_{rI} = \frac{a^2 b^2 p_o}{r^2 (a^2 - b^2)} - \frac{p_o b^2}{(b^2 - a^2)} = -\frac{5}{2} \frac{a^2 b^2}{r^2 (b^2 - a^2)} + \frac{5}{2} \frac{b^2}{(b^2 - a^2)}$$

$$\sigma_\theta = -\frac{1}{r^2} \frac{a^2 b^2 (p_o - p_i)}{(b^2 - a^2)} + \frac{p_i a^2 - p_o b^2}{(b^2 - a^2)}$$

$$\sigma_{rI} = \frac{5}{2} \frac{1}{1 - \frac{a^2}{b^2}} \left[ 1 - \frac{a^2}{r^2} \right] \quad \text{let } b \rightarrow \infty \quad \sigma_{rI} = \frac{5}{2} \left[ 1 - \frac{a^2}{r^2} \right]$$

$$\sigma_{\theta I} = \frac{5}{2} \left[ 1 + \frac{a^2}{r^2} \right] \quad \tau_{r\theta} = 0$$

### PART II

$$\nabla^4 \phi = \frac{\partial^4 \phi}{\partial r^4} + \frac{2}{r} \frac{\partial^3 \phi}{\partial r^3} - \frac{1}{r^2} \frac{\partial^2 \phi}{\partial r^2} + \frac{2}{r^2} \frac{\partial^4 \phi}{\partial r^2 \partial \theta^2} + \frac{1}{r^3} \frac{\partial \phi}{\partial r} - \frac{2}{r^3} \frac{\partial^3 \phi}{\partial r \partial \theta^2} + \frac{4}{r^4} \frac{\partial^2 \phi}{\partial \theta^2} + \frac{1}{r^4} \frac{\partial^4 \phi}{\partial \theta^4} = 0$$

Assume  $\phi = f(r) \cos 2\theta$  using  $\sigma_r = \frac{1}{r} \frac{\partial \phi}{\partial r} + \frac{1}{r^2} \frac{\partial^2 \phi}{\partial \theta^2}$

$$\cos 2\theta \left[ \frac{\partial^4 f(r)}{\partial r^4} + \frac{2}{r} \frac{\partial^3 f(r)}{\partial r^3} - \frac{1}{r^2} \frac{\partial^2 f(r)}{\partial r^2} - \frac{8}{r^2} \frac{\partial^2 f(r)}{\partial r^2} + \frac{1}{r^3} \frac{\partial f(r)}{\partial r} + \frac{8}{r^3} \frac{\partial f(r)}{\partial r} - \frac{16}{r^4} f(r) + \frac{16}{r^4} f(r) \right] = 0$$

$$\frac{\partial^4 f(r)}{\partial r^4} + \frac{2}{r} \frac{\partial^3 f(r)}{\partial r^3} - \frac{9}{r^2} \frac{\partial^2 f(r)}{\partial r^2} + \frac{9}{r^3} \frac{\partial f(r)}{\partial r} = 0$$

let  $r = e^t$

$$r^4 \frac{\partial^4 f(r)}{\partial r^4} = D(D-1)(D-2)(D-3)$$

$$r^3 \frac{\partial^3 f(r)}{\partial r^3} = D(D-1)(D-2)$$

$$r^2 \frac{\partial^2 f(r)}{\partial r^2} = D(D-1)$$

$$r \frac{\partial f(r)}{\partial r} = D$$

$$D(D-1)D(D-2)(D-3) f(r) + 2D(D-1)(D-2) f(r) - 9D(D-1) f(r) + 9D f(r) = 0$$



Which reduces to  $[D^4 - 4D^3 - 4D^2 + 16D]f(r) = 0$

let  $f = e^{mt}$   $D = \frac{d}{dt}$  then  $\frac{d^4 f(r)}{dt^4} - 4\frac{d^3 f(r)}{dt^3} - 4\frac{d^2 f(r)}{dt^2} + 16\frac{df(r)}{dt} = 0$

$m^4 - 4m^3 - 4m^2 + 16m = 0$   $m(m^3 - 4m^2 - 4m + 16) = 0$

$m = 0, 2, -2, 4$   $f(r) = Ae^{2t} + Be^{4t} + Ce^{-2t} + D$

$r = e^t$ ,  $f(r) = Ar^2 + Br^4 + \frac{C}{r^2} + D$

$\phi = \cos 2\theta [Ar^2 + Br^4 + \frac{C}{r^2} + D]$ ,  $\frac{1}{r} \frac{\partial \phi}{\partial r} = \cos 2\theta [2A + 4Br^2 - \frac{2C}{r^4}]$

$\frac{1}{r^2} \frac{\partial^2 \phi}{\partial r^2} = -\cos 2\theta [4A + 4Br^2 + \frac{4C}{r^4} + \frac{4D}{r^2}]$

$\sigma_r = \frac{1}{r} \frac{\partial \phi}{\partial r} + \frac{1}{r^2} \frac{\partial^2 \phi}{\partial r^2} = -\cos 2\theta [2A + \frac{6C}{r^4} + \frac{4D}{r^2}]$

$\sigma_\theta = \frac{\partial^2 \phi}{\partial r^2} = \cos 2\theta [2A + 12Br^2 + \frac{6C}{r^4}]$

$\tau_{r\theta} = -\frac{\partial}{\partial r}(\frac{1}{r} \frac{\partial \phi}{\partial r}) = 2 \sin 2\theta [A + 3Br^2 - \frac{3C}{r^4} - \frac{D}{r^2}]$

BOUNDARY CONDITIONS  $\sigma_r|_{r=a} = 0$   $\tau_{r\theta}|_{r=a} = 0$

if  $b \gg a$   $\sigma_r|_{r=b} = \frac{S}{2} \cos 2\theta$   $\tau_{r\theta}|_{r=b} = -\frac{S}{2} \sin 2\theta$

1]  $2A + \frac{6C}{a^4} + \frac{4D}{a^2} = 0$  2]  $2A + \frac{6C}{b^4} + \frac{4D}{b^2} = -\frac{S}{2}$

3]  $2A + 6Ba^2 - \frac{6C}{a^4} - \frac{2D}{a^2} = 0$  4]  $2A + 6Bb^2 - \frac{6C}{b^4} - \frac{2D}{b^2} = -\frac{S}{2}$

as  $b \rightarrow \infty$ ,  $A \rightarrow -\frac{S}{4}$   $\therefore \boxed{A \approx -\frac{S}{4}}$  from 2]

as  $b \rightarrow \infty$ ,  $-\frac{S}{2} + 6Bb^2 - \frac{1}{\infty} - \frac{1}{\infty} = -\frac{S}{2}$ ,  $6Bb^2 = 0$   $\therefore \boxed{B \approx 0}$  from 4]

$\frac{6C}{a^4} + \frac{4D}{a^2} = \frac{S}{2}$  or  $6C + 4Da^2 = \frac{S}{2}a^4$  from 1]

$-\frac{6C}{a^4} - \frac{2D}{a^2} = \frac{S}{2}$  or  $-6C - 2Da^2 = \frac{S}{2}a^4$  from 3]

$2Da^2 = Sa^4$   $\boxed{D = \frac{Sa^2}{2}}$ ,  $\boxed{C = -\frac{Sa^4}{4}}$

$\sigma_r = -\cos 2\theta [-\frac{S}{2} + \frac{6}{r^4}(-\frac{Sa^4}{4}) + \frac{4}{r^2}(\frac{Sa^2}{2})]$

$\sigma_\theta = \cos 2\theta [-\frac{S}{2} + \frac{6}{r^4}(-\frac{Sa^4}{4})]$

$\sigma_{rII} = S \cos 2\theta [\frac{1}{2} + \frac{3}{2} \frac{a^4}{r^4} - \frac{2a^3}{r^2}]$   $\sigma_{\theta II} = -S \cos 2\theta [\frac{1}{2} + \frac{3}{2} \frac{a^4}{r^4}]$

$\tau_{r\theta II} = -S \sin 2\theta [\frac{1}{2} - \frac{3}{2} \frac{a^4}{r^4} + \frac{a^2}{r^2}]$





## SUPERIMPOSING PART I AND PART II

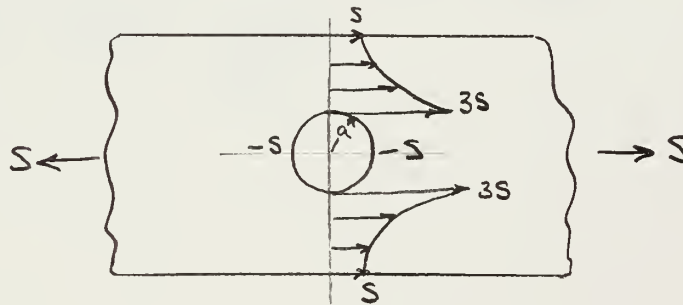
$$\sigma_r = \frac{S}{2} \left[ 1 - \frac{a^2}{r^2} \right] + \frac{S}{2} \left[ 1 + \frac{3a^4}{r^4} - \frac{4a^2}{r^2} \right] \cos 2\theta$$

$$\sigma_\theta = \frac{S}{2} \left[ 1 + \frac{a^2}{r^2} \right] - \frac{S}{2} \left[ 1 + \frac{3a^4}{r^4} \right] \cos 2\theta$$

$$\tau_{r\theta} = -\frac{S}{2} \left[ 1 - \frac{3a^4}{r^4} + \frac{2a^2}{r^2} \right] \sin 2\theta$$

$$\sigma_r|_{r=a} = 0 \quad \sigma_\theta|_{r=a} = S(1 - 2\cos 2\theta) \quad \tau_{r\theta}|_{r=a} = 0$$

$$\sigma_\theta|_{r=a, \theta=\frac{\pi}{2}} = S - 2S(-1) = 3S \quad \sigma_\theta|_{r=a, \theta=0} = -S$$



At the hole perimeter, the only  $\sigma$  is  $\sigma_\theta$ . The elastic strain

$$\epsilon_3 = \frac{1}{E} \left[ \cancel{\sigma_r} - \nu(\cancel{\sigma_r} + \sigma_\theta) \right] = -\frac{\nu}{E} \sigma_\theta = \frac{-.33}{10.5 \times 10^6} \sigma_\theta = -3.14 \times 10^{-8} \sigma_\theta$$

For  $\sigma_\theta = 10,950$  psi,  $\epsilon_3 = (-.314)(10,950)10^{-7} = -348 \mu\text{in/in}$

One fringe [App. 1] for 10,950 psi.

For plate with  $b=4$ ,  $a=.067$ ,  $E=10.5 \times 10^6$ ,  $\sigma_\theta = 10,950$

$$\text{Area} = (4.000 - .067)(.0625) = .2455$$

$$F = \sigma A = (10,950)(.2455) = 2685 \text{ lbs.}$$

LOAD REQUIRED TO PRODUCE ONE FRINGE IS 2685 lbs.



#### APPENDIX 4

##### EVALUATION OF CONSTANT K FOR PROPAGATION RATE EXPRESSIONS OF FIGURES 6 AND 7

For the central slot:

$$V_c = K_c \sigma^5$$

$$\text{at } \sigma = 10 \text{ KSI} \quad V = .016 \text{ in}^3/\text{sec}$$

$$K_c = V_c / \sigma^5 = \frac{.016}{10^5} = .0016 \frac{\text{in}^3/\text{sec}}{\text{KSI}^5}$$

For the edge slot:

$$V_e = K_e \sigma^5$$

$$\text{at } \sigma = 10 \text{ KSI} \quad V = .034 \text{ in}^3/\text{sec.}$$

$$K_e = .0034 \frac{\text{in}^3/\text{sec}}{\text{KSI}^5}$$















thesT824

Investigation of strain distribution aro



3 2768 001 88856 3

DUDLEY KNOX LIBRARY